The Pennsylvania State University
The Graduate School

DEVELOPMENT AND CHARACTERIZATION OF ELECTROCHEMICAL BIOSENSORS BASED ON ELECTRODEPOSITED COPPER-NICKEL AND LASER WRITTEN PLATINUM ELECTRODES

A Thesis in
Electrical Engineering
by
Lindsey Goodnight

Submitted in Partial Fulfillment
of the Requirements
for the Degree of

Master of Science

August 2021

The thesis of Lindsey Goodnight was reviewed and approved by the following:

Aida Ebrahimi
Assistant Professor of Electrical Engineering
Thesis Advisor

Timothy Kane
Professor of Electrical Engineering

Kultegin Aydin
Professor of Electrical Engineering
Head of the Department of Electrical Engineering

Abstract

The ability to perform diagnostic tests quickly in non-laboratory settings using point-of-care (PoC) testing devices is of great interest for personalized health monitoring. Electrochemical sensors, in particular, are of interest for PoC testing devices as they can be portable and have quick response time. Non-enzymatic electrochemical testing using engineered electrodes have attracted increasing attention in the bioisensing community since enzymes can be difficult to replicate. Enzymes can be susceptible to environmental conditions such as temperature, pH, humidity, etc. In this work, we develop and investigate different inorganic materials based on transition metals to be used as disposable electrochemical biosensors for glucose and hydrogen peroxide with the potential for in vitro PoC diagnostic applications. The first material explored is phosphate buffer saline (PBS) treated electrodeposited copper-nickel (Cu-Ni) structures for detection of glucose. The PBS treatment and a two-step annealing process enhance the electrode stability and the sensitivity to glucose in a neutral pH in comparison to the Cu-Ni alone. The sensitivity, selectivity, and lifetime were explored through cyclic voltammetry (CV). The of limit detection of this material was 1 nM in neutral pH in 0.1 M Na_2SO_4. Material characterizations were done with Scanning Electron Microscopy (SEM), X-Ray Photoelectron Spectroscopy (XPS), and Energy-dispersive X-ray spectroscopy (EDS). The second material explored is laser-written metals, in particular platinum. By applying a laser onto a solution containing metal ions, the thermal energy from the laser decomposes the liquid and results in deposition of a metal film onto a substrate. The sensitivity for various salt concentrations and the effect of applied frequency were tested using square wave voltammetry (SWV). XPS and SEM were used to characterize the material. The limit of detection was found to be 5 fM in PBS. Both deposition methods, i.e. electrodeposition and laser-writing, are low-cost and scalable and can enable fabricating disposable electrochemical sensors for PoC testing.

Table of Contents

List of Figures vi

List of Tables x

Acknowledgments xi

Chapter 1
Introduction to Biosensors 1
1.1 Classification of Biosensors . . . 1
1.2 Electrochemical Biosensors . . . 2
1.2.1 Principle of Operation . . . 2
1.2.2 Cyclic Voltammetry . . . 3
1.2.3 Square Wave Voltammetry . . . 6
1.3 Outline of Thesis . . . 7
1.4 List of Associated Publications . . . 8

Chapter 2
PBS-treated Electrodeposited Cu-Ni Structures for Electrochemical Detection of Glucose in Neutral pH 9
2.1 Introduction . . . 9
2.2 Experimental procedure and Results . . . 11
2.2.1 Electrodeposition of nickel (Ni) . . . 11
2.2.2 Electrodeposition of copper (Cu) . . . 12
2.2.3 Electrochemical characterization . . . 12
2.2.4 Sensor Development and Characterization . . . 13
2.2.5 Sensor performance: sensitivity, selectivity, and stability . . . 17
2.3 Conclusion . . . 20

Chapter 3
Developing Hydrogen Peroxide Sensors using Laser Written Platinum Electrodes 21
3.1 Introduction . . . 21
3.2 Experimental Procedure and Results . . . 22
3.2.1 Materials and Methods . . . 22

3.2.1.1 Laser Writing Method 22
3.2.1.2 Material Characterization 23
3.2.1.3 Electrochemical Testing Method 24
3.2.2 Characterizing laser-written Pt working electrodes for sensing H_2O_2 24
3.2.2.1 Studying the effect of salt concentration on sensitivity . 24
3.2.2.2 Studying the effects of substrate and precursor salt concentration on sensitivity 26
3.2.2.3 Studying the effects of background medium and SWV frequency on sensitivity 26
3.2.2.4 Studying the lifetime and effects of dissolved oxygen . . 27
3.2.2.5 Studying the effect of interfering analytes 28
3.2.2.6 Preliminary fabrication of an on-chip sensor 29
3.3 Conclusion 31

Chapter 4
Summary and Future Work **33**

Appendix A
Optimization of the Processing Steps for Developing PBS-Cu-Ni Electrodes **35**

Appendix B
Characterization of Laser-written Silver and Carbon Pseudo Reference Electrodes **38**

Bibliography **40**

List of Figures

1.1 **The general components of biosensors**, include a target analyte detection by a corresponding receptor biorecognition followed by an input signal transducer method that creates an output signal. 2

1.2 **The growth of the point-of-care biosensors market** has been rapid in the past few years. Source: www.grandviewresearch.com. 3

1.3 **Differences between Faradaic and non-Faradaic processes**, Faradaic processes study the charge conversion and non-Faradaic processes study the charge storage. Adapted from Ref. [9] (arXiv:1809.02930). 4

1.4 **Three-electrode system**, the working electrode (WE), counter electrode (CE), and reference electrode (RE) are shown. The voltage is applied between the WE and RE, and the current is measured between the We and CE. 5

1.5 **Example CV signals** are shown, a) shows the applied voltage signal, b) shows several CV curves of a redox couple (5 mM ferri/ferrocyanide) in PBS (pH 7.4) by sweeping the voltage from -0.5 V to 0.5 V at a scan rate of 50 mVs^{-1} with a working of platinum working electrode. 6

1.6 **Example SWV signals,** a) sample applied voltage signal for SWV, b) reduction SWV for 500 nM H_2O_2 in PBS sweeping from 0.25 V to -0.25 V, step size 0.01 V, pulse size (amplitude) of 0.025 V, and frequency of 3 Hz using a laser-written Pt electrode to be discussed in Chapter 3. 7

2.1 **Electrodeposition set up.** The reference (ref.)/counter electrode was a stainless steal plate, working electrode was a 1 cm by 1 cm Cr/Au sample. 12

2.2 **Electrodeposition curves** a) the potential curve during the Ni deposition b) the potential curve during the Cu deposition. 13

2.3 **Fabrication schematic** a) Electrodeposition of nickel (Ni) on thin film gold (Au) layer deposited on glass substrate. b) Copper (Cu) electrodeposition at 50°C for 2 min. c) The two-step annealing process, with Step 1 in air at room-temperature for four days, followed by Step 2 at 150°C for 1 hour. d) Electrochemical treatment of Cu-Ni electrodes in PBS using cyclic voltammetry (CV). At least 45 scans are performed until CV curves are stabilized. The inset shows representative CV curves. 14

2.4 **SEM imgaes** of a) Cu-Ni electrode before the two-step annealing process, b) Cu-Ni electrode after the two-step annealing, c) PBS-treated Cu-Ni (PBS-Cu-Ni) electrode. Scale bar: 500 nm. 14

2.5 **Morphology and elemental composition of PBS-Cu-Ni electrode.** EDS maps for a) chlorine (Cl), b) copper (Cu), c) phosphorous (P), d) oxygen (O). e) The corresponding SEM image. f) Atomic percentage (AT%) for the elemental composition of PBS-Cu-Ni. Scale bar: 5 µm. . . 16

2.6 **Cyclic voltammogram (CV) curves** of a) 5 mM glucose in 0.1 M Na_2SO_4 for Ni, Cu-Ni, and PBS-Cu-Ni electrodes. b) CV curves at different scan rates from 10 to 500 mVs^{-1} of 1 mM Glucose in 0.1 M Na2SO4. The inset shows the relationship between the oxidation (black curve) and reduction (red curve) peak current vs. the square root of the scan rate. 16

2.7 **Sensor sensitivity and selectivity**. Cyclic voltammograms (CV) curves of a) peak oxidation current at 0.2 V normalized by the baseline current, I_0, for various glucose concentrations in 0.1 M Na2SO4 (pH 6.4). The error bars depict the standard errors with n = 3. CV curves for b) 1% and 3% diluted artificial saliva with 65 µM, UA is 175.4 µM and AA is 600 nM into Na_2SO_4 normalized to the baseline of artificial saliva and Na_2SO_4. 18

2.8 **PBS treatment is essential for sensor stability**. The oxidation current on day seven normalized to the initial signal (on day one) over the entire sensor dynamic range (5 nM- 20 mM). The sample was stored in ambient condition. 18

3.1 **Fabrication steps to create laser-written metals.** a) The laser writing setup, b) the laser writing pattern. These figures are provided by Alex Castonguay. 23

3.2 **SEM images of LW Pt samples** a) scale bar 1 µm, b) scale bar 5 µm. These figures are provided by Alex Castonguay. 23

3.3 **XPS of LW Pt samples.** This data is provided by Alex Castonguay. . 24

3.4 **The testing setup** with Pt CE, Ag/AgCl reference electrode, and LW-Pt as the WE. 25

3.5 **The current-voltage curves** obtained with various concentrations of H_2O_2 in PBS using a) SWV, b) CV. SWV yields a higher sensitivity and the analytical method of choice in this work.. 25

3.6 **The effect of the precursor salt concentration and FTO vs. non-FTO substrates.** a) response to H_2O_2 in PBS printed using precursors with different salt concentrations on FTO glass (0.5 M slope = -0.73, 0.05 M slope = -0.39, 0.25 slope = -0.27), b) response to H_2O_2 using PBS in 0.25 M salt on non-FTO glass (slope = -0.66). 26

3.7 **The effect of different background solutions and SWV frequency**. a) various concentrations of H_2O_2 in PBS or 100 mM KCl were studied, b) the slope (sensitivity) of sensors with different exposed The inset shows the magnified view of the area. signal using "Small" sensor surface area. . 27

3.8 **Sensor lifetime and effect of dissolved oxygen.** a) The SWV response of the same sample over multiple days tested with PBS and PBS with 5 nM H_2O_2 at 3 Hz b)the response to H_2O_2 N_2-purged to remove all dissolved O_2 in the solution on FTO glass as the substrate. 28

3.9 **Studying the sensor lifetime and effect of sample washing.** a) The SWV signal in blank solution (PBS) in the presence of dissolved oxygen scan with samples cleaned in PBS (Trial 1-3) or 99% IPA and PBS (Trial 4), b) sensor response to 500μM, 5 nM, and 500 nM H_2O_2 in PBS with samples cleaned through Trial 1-4. 29

3.10 **Studying the sensor response to interference.** The tests were done in PBS on borosilicate glass and the curves are subtracted from a baseline. 30

3.11 **Studying on-chip fabrication** a) The printer design of the chip and electrode dimension. b) The chip attached to a potentiostat. 31

A.1 a) Electrodeposited Cu-Ni before testing. b) Electrodeposited Cu-Ni after testing. 35

A.2 a) The various timelines tested. Annealing was done at 150°C. b) The response in comparison of the different timelines on Day 4 testing in Na_2SO_4 36

A.3 **Water on PBS-Cu-Ni** 5 µL of water dropped on the surface. 37

B.1 **The OCP laser-written C and Ag non-FTO glass.** Mean, standard deviation, and standard error applies to the whole scan. 39

List of Tables

2.1 **EDS data** comparing the elemental composition of different steps of fabrication. 15

2.2 **Comparable glucose sensors** are listed displaying various characteristics of each sensor. NPs: nanoparticles, CNTs: carbon nanotubes, GCE: glassy carbon electrode, MWCNTs: multi-walled carbon nanotubes, PGE: Pencil graphene electrode, SWCNT: single-walled carbon nanotube, PPy: polypyrrole. 19

3.1 **Comparable H_2O_2 sensors** are listed displaying various characteristics of each sensor.NPs: nanoparticles, SPCE: screen-printed carbon electrodes , GCE: glassy carbon electrode, RGO: reduced graphene oxide, CNF: nanoporous carbon nanofibers, ITO: indium tin oxide, PPy: polypyrrole, N_2-sat: nitrogen saturated. 32

Acknowledgments

I want to thank Dr. Aida Ebrahimi for her guidance and support through out my undergraduate studies and graduate studies at Penn State. Dr. Ebrahimi has been an incredible role model. I would not be where I am without her support.

I also want to thank Dr. Timothy Kane. Dr. Kane has been instrumental with starting my research career. He has been a great support in exploring my career.

I want to thank Ebrahimi lab members, in particular Derrick Butler, Adam Bolotsky, Chengye Dong, and Keren Zhou. They have helped me by training me and supported me through my studies.

I would like to thank Dr. Zarzar's group, Alex Castonguay in particular, for preparing the laser-written materials.

I want to thank the Erickson Discovery Grant and the Humanitarian Award by the Materials Research Institute for partial financial support for the research presented in this thesis.

Chapter 1
Introduction to Biosensors

Biosensors are devices that detect biological materials (such as small molecules, nucleic acids, proteins, whole cells, etc.) and convert the response into a more analytically convenient signal [29, 46] Most biosensors consist mainly of two key elements: a biorecognition component, and a transducer component. The biorecognition component generally contains receptors leading to change of sensor signal with a high degree of selectivity for the target analyte to be measured and translate information from the biochemical domain into a chemical/physical output signal. [29] The transducer component of the sensor transforms the output signal from the biological recognition component into an electrical signal.

1.1 Classification of Biosensors

Biosensors are often classified according to the biological recognition component (e.g. aptamer-sensors), or the detection method (e.g. impedimetric sensors), or as a combination of the two (e.g. amperometric-enzyme sensors). Fig 1.1 shows the various types of analytes (cell cultures, human samples), biorecognition component (cells, antibodies), and transducers (optical, electrochemical). Recent trends in healthcare is progressing toward personalized medicine, continuous monitoring, and point-of-care (PoC) diagnostics. The rapid growth of the PoC device market is shown in Fig. 1.2, and the market is projected to grow in the next 6 years. The sensors developed in this thesis measure electrochemical signals using electrochemical techniques, which compared to other methods have displayed significant potential for rapid response, miniaturization, and portability for PoC settings. [17]

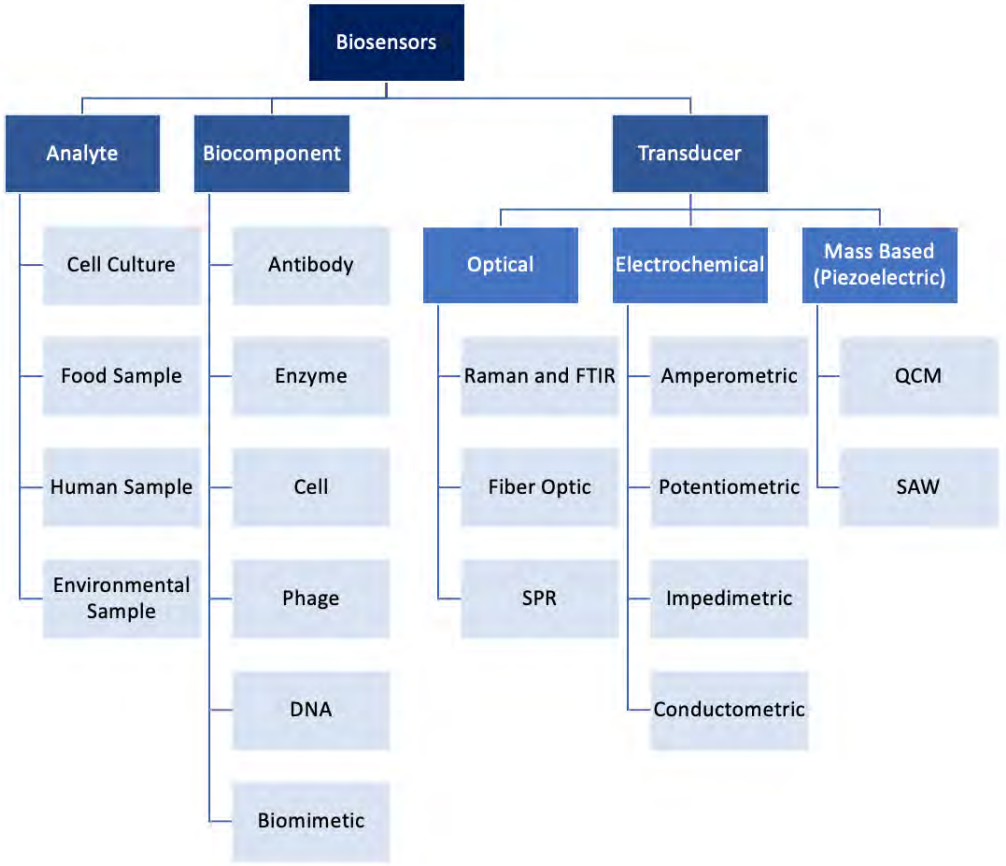

Figure 1.1. The general components of biosensors, include a target analyte detection by a corresponding receptor biorecognition followed by an input signal transducer method that creates an output signal.

1.2 Electrochemical Biosensors

1.2.1 Principle of Operation

There are two main processes that occur at the electrode of electrochemical sensors: Faradaic and non-Faradaic. Non-Faradaic processes study the storage of charge on the electrodes. The capacitive component of the electrode can change through adsorption and desorption. [9] Faradaic processes study the charge transfer at the interface, generally from reduction and oxidation (redox) reactions. [9] Fig.1.3 shows the interface between the electrode and electrolyte with respect the two processes.

Faradaic electrochemical sensors work by detecting changes in Faradaic current, through either amperometric or potentiometric (also called voltammetric) techniques, or the interfacial impedance, using electrochemical impedance spectroscopy (EIS). [76]

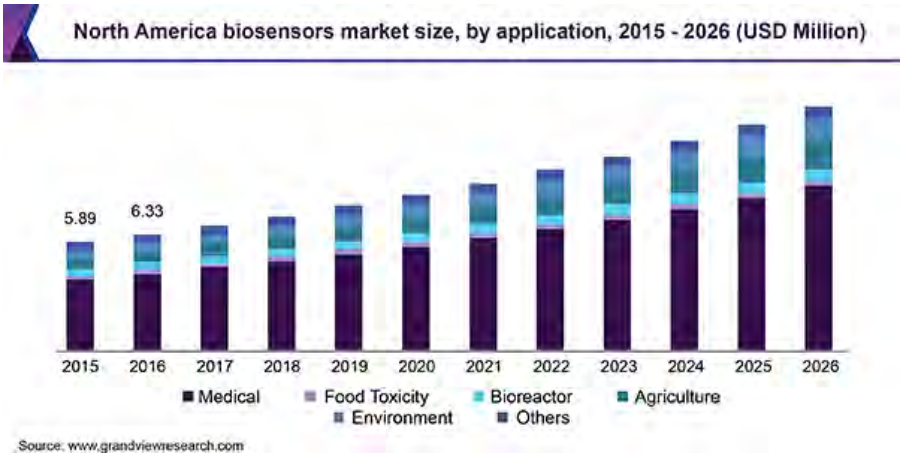

Figure 1.2. The growth of the point-of-care biosensors market has been rapid in the past few years. Source: www.grandviewresearch.com.

These types of tests are typically done with a three-electrode system. Fig. 1.4 shows a general set up for a three-electrode system. The working electrode (WE) is the material being studied. Another electrode is the reference electrode (RE). The RE is used to apply and maintain a voltage at the WE. As a result, a characteristic of RE is that no current occurs over a wide range of voltages. This material is ususally Ag/AgCl or Hg/Hg_2Cl_2. The third electrode, counter electrode (CE), is used to measure the current that results from the applied voltage.

Amperometry and voltammetry involve measurement of the current resulting from the electrochemical oxidation or reduction of an electro-active species due to the regulation of the electrode potential. Amperometry is conducted by applying a fixed potential while the resulting current is measured over time, whereas for voltammetry the resulting current is measured for varying potential. Commonly used electrochemical techniques include chronoamperometry, differential pulse voltammetry (DPV), cyclic voltammetry (CV), square-wave voltammetry (SWV), and electrochemical impedance spectroscopy (EIS). In the work, CV and SWV are implemented.

1.2.2 Cyclic Voltammetry

Cyclic voltammetry (CV) is a very common type of electrochemical measurement to study electron transfer upon reduction or oxidation (redox) of an analyte. This method is used extensively throughout this research. CV is performed by sweeping the applied voltage from the starting potential to a switching potential and from the switching point to the starting potential, as seen in Fig. 1.5a. Full redox cycle is created by linearly

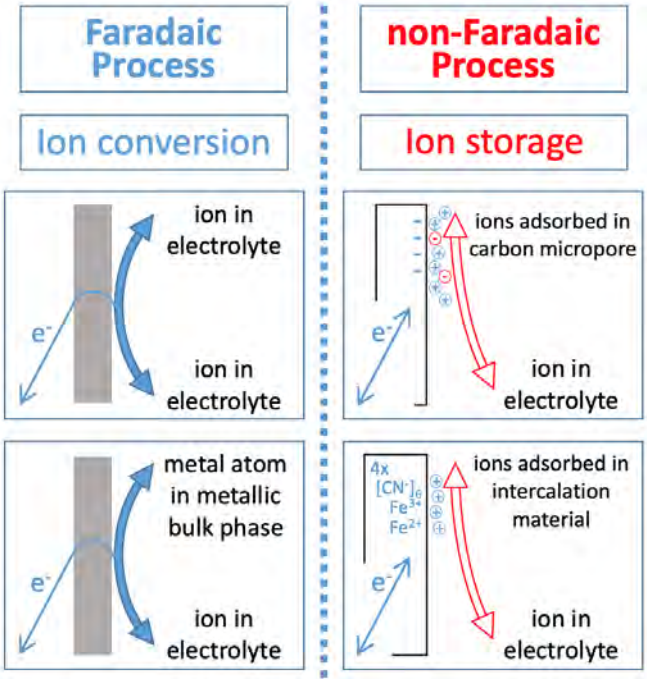

Figure 1.3. Differences between Faradaic and non-Faradaic processes, Faradaic processes study the charge conversion and non-Faradaic processes study the charge storage. Adapted from Ref. [9] (arXiv:1809.02930).

sweeping from the higher voltage first to the lower voltage (reduction) and then from the lower voltage to the higher voltage (oxidation). An example of a CV curve can be seen in Fig 1.5b.

The resulting current is governed by the electron transfer resulting from redox reactions. Generally, if the reactions are reversible, a "duck" shape curve is observed. This "duck" shape is from the Nernst Equation as shown in Eq.1.1. Assumptions made for Nernstian systems is fast reaction kinetics. A fast reaction means that oxidation or reduction happens as fast as the analyte can diffuse to the electrode. [8] Where R is the universal gas constant, T is temperature, n is the number of electrons, $C_O(0,t)$ is the concentration of the oxidative species, $C_R(0,t)$ is the concentration of the reductive species, and F is Faraday's constant.

$$E = E^0 + \frac{RT}{nF} \ln \frac{C_O(0,t)}{C_R(0,t)} \tag{1.1}$$

A convenient way to rewrite Eq. 1.1 is:

$$\theta = \frac{C_O(0,t)}{C_R(0,t)} = \exp\left[\frac{nF}{RT}(E - E^{0'})\right] \tag{1.2}$$

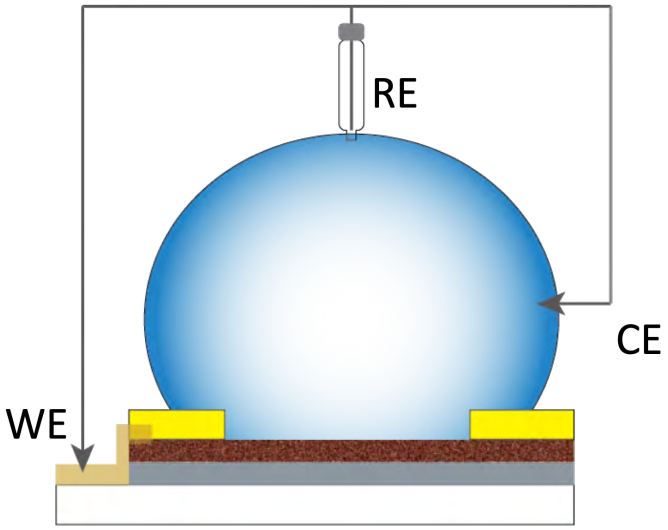

Figure 1.4. Three-electrode system, the working electrode (WE), counter electrode (CE), and reference electrode (RE) are shown. The voltage is applied between the WE and RE, and the current is measured between the We and CE.

Since the voltage is swept linearly at a specified scan rate (ν), the potential can be modeled as:

$$E(t) = E_i - \nu t \tag{1.3}$$

Eq. 1.2 can be rewritten with Eq. 1.3. The boundary condition can then be written as:

$$\frac{C_O(0,t)}{C_R(0,t)} = \exp\left[\frac{nF}{RT}(E_i - \nu t - E^{0'})\right] = \theta S(t) \tag{1.4}$$

Where $S(t) = e^{-\sigma t}$, $\theta = \exp\left[(nF/RT)(E_i - E^{0'})\right]$, and $\sigma = (NF/RT\nu)$. By taking the Laplace transformation of the initial and semi-infinite conditions lead to:

$$C_O(0,t) = C_O^* - [nFA(\pi D_O)^{1/2}]^{-1} \int_0^t i(\tau)(t-\tau)^{-1/2} d\tau \tag{1.5}$$

Where C_O^* is the bulk concentration of oxidative species. With evaluating the integral and substitutions an equation for current is found in Eq. 1.6. Where χ is a constant that is normally looked up in a table and D_O is the diffusion constant (cm^2/s).

$$i = nFAC_O^*(\pi D_O \sigma)^{1/2}\chi(\sigma t) \tag{1.6}$$

From Eq. 1.6 the peak current can be derived when $\pi^{1/2}\chi(\sigma t)$ is at maximum

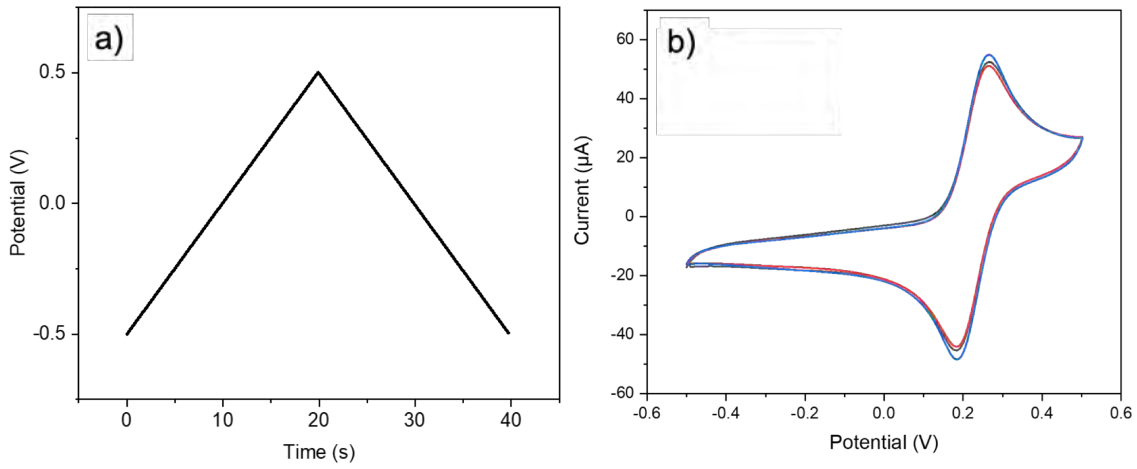

Figure 1.5. Example CV signals are shown, a) shows the applied voltage signal, b) shows several CV curves of a redox couple (5 mM ferri/ferrocyanide) in PBS (pH 7.4) by sweeping the voltage from -0.5 V to 0.5 V at a scan rate of 50 mVs^{-1} with a working of platinum working electrode.

($\pi^{1/2}\chi(\sigma t) = 0.4463$). [8] With all of the constants computed the peak equation is shown in Eq. 1.7.

$$i_p = (2.69 \times 10^5) n^{3/2} A D_O^{1/2} C_O^* \nu^{1/2} \tag{1.7}$$

The "duck" shape occurs in the Nernstian system where there is a peak in both forward (reduction) and backward (oxidation) sweep. If the reaction is mass-transfer limited the i_p should be identical. [8]

1.2.3 Square Wave Voltammetry

Square Wave Voltammetry is another commonly used electrochemical method for detection of redox reactive species. It is similar to CV where a voltage is applied but instead of sweeping voltage, a square wave is applied as shown in Fig. 1.6. Adjustable parameters of SWV are start potential, end potential, amplitude, and frequency.

This type of voltammetry has an advantage over CV because it can suppress the background signal better, and much lower concentration can be examined. Samples of the current is measured for both the forward and reverse reaction, and Δi is plotted. This subtraction leads to the background suppression. [8]

One study conducted by Fang C. et. al. utilized SWV for a glucose non-enzymatic

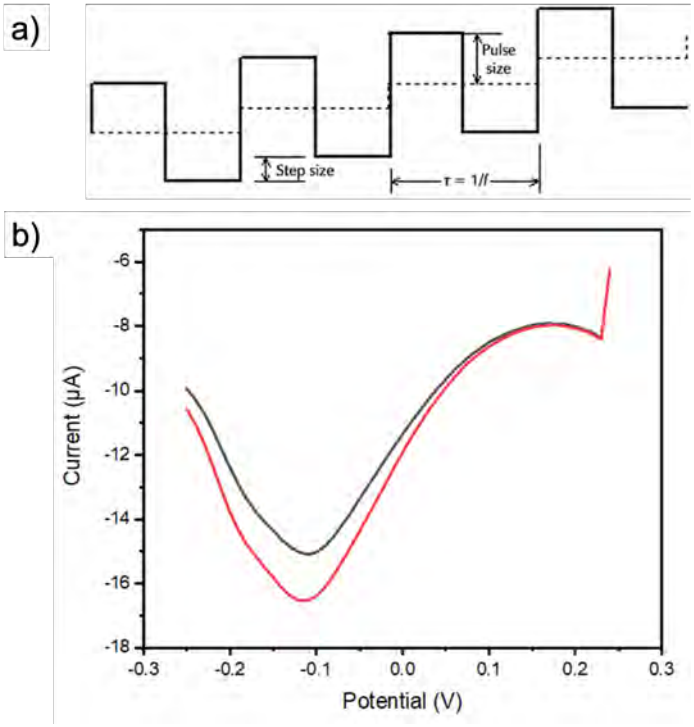

Figure 1.6. Example SWV signals, a) sample applied voltage signal for SWV, b) reduction SWV for 500 nM H_2O_2 in PBS sweeping from 0.25 V to -0.25 V, step size 0.01 V, pulse size (amplitude) of 0.025 V, and frequency of 3 Hz using a laser-written Pt electrode to be discussed in Chapter 3.

electrochemical sensor. An alkaline solution was used to have a linear range 5.0–120 µM of glucose with a limit of detection of 0.2 µM. [22]

1.3 Outline of Thesis

This thesis demonstrates the development and characterization of electrochemical biosensors using electroplated copper-nickel and laser written platinum. The outline of the thesis is as follows:

- Chapter 2 discusses development and application of PBS-treated Cu-Ni structures for non-enzymatic glucose detection in neutral pH. Section 2.1 introduces the importance of detecting glucose and provides a review on the current methods reported for glucose detection. Section 2.2 details the sensor fabrication process, characterization, experimental procedure, and testing results. Section 2.3 summarizes the experimental findings and provides a brief overview of the future work. The contents of Chapter 2 is adapted/reproduced from Ref. [26] (to be submitted).

- Chapter 3 discusses the development of hydrogen peroxide sensors using laser-written platinum. Section 3.1 introduces the importance of detecting hydrogen peroxide and provides a brief review on the current methods of detecting H_2O_2. Section 3.2 details the sensor fabrication procedure, characterization, experimental procedure, and testing results. Section 3.3 summarizes the experimental findings and provides a brief overview of the future work.The contents of Chapter 3 is adapted/reproduced from Ref. [82]

- Chapter 4 summarizes the findings in this thesis and the future outlook.

1.4 List of Associated Publications

Journal

1. **L. Goodnight**, D. Butler, T. Xia A. Ebrahimi, PBS-treated Electrodeposited Cu-Ni Structures Enable Highly Sensitive Electrochemical Detection of Glucose in Neutral pH, to be submitted.

2. A. Castonguay, **L. Goodnight**, A. Ebrahimi, L. Zarzar, Detection of Hydrogen Peroxide Down to Femtomolar Level using Patternable Laser Written Platinum on Glass, to be submitted.

3. D. Butler, N. Goel, **L. Goodnight**, S. Tadigadapa, and A. Ebrahimi, Detection of Bacterial Metabolism in Lag-Phase using Impedance Spectroscopy of Agar-integrated 3D Microelectrodes, Biosensors and Bioelectronics 129 (2019) 269-276.

4. A. Ebrahimi, K. Zhang, C. Dong, S. Subramanian, D. Butler, A. Bolotsky, **L. Goodnight**, Y. Cheng, J. A. Robinson*, (2019). FeSx-graphene heterostructures: Nanofabrication-compatible catalysts for ultra-sensitive electrochemical detection of hydrogen peroxide. Sensors and Actuators B: Chemical, 285, 631-638.

Conference

1. **L. Goodnight**, D. Butler, A. Ebrahimi Non-Enzymatic Detection of Glucose in Neutral pH using PBS-Activated Cu-Ni Electrodes, Materials Day (October 2020, University Park, PA).

Chapter 2
PBS-treated Electrodeposited Cu-Ni Structures for Electrochemical Detection of Glucose in Neutral pH

This chapter discusses development and application of PBS-treated electrodeposited Cu-Ni to detect glucose in neutral pH. In Section 2.1 the importance of glucose detection is discussed. Then the fabrication process, characterization, experimental procedure, and results are explained in Section 2.2. Finally in Section 2.3, the findings of the experiments are summarized. Some parts of the results in this chapter were presented in Ref. [26]. The detailed report will be submitted for review in a journal publication.

2.1 Introduction

Diabetes is a worldwide health problem and one of the leading causes of death and disability [58, 77]. As such, patients with diabetes are clinically advised to monitor their glucose levels regularly [58, 72]. Treatment for diabetes requires compact and accurate glucose monitoring, which has made developing glucose sensors a highly active research area in the biosensor community, especially in point-of-care testing domain. Conventional enzyme-based sensors based on glucose oxidase (GOx) offer superior selectivity and good sensitivity for detecting glucose in physiological pH. However, enzymes suffer from stability issues due to their sensitivity to environmental pH, temperature, humidity, and interference of some electro-oxidizable species because of their enzymatic nature [3, 25, 36, 37, 55, 71, 86]. Moreover, enzymatic sensors are limited by the enzyme leaching,

electrode replacement [63], and are not amenable for electrode miniaturization for high throughput readout of small sample volumes [10].

To address these challenges, non-enzymatic glucose sensors have been developed based on electro-oxidation of glucose which can be detected optically or electrochemically. Optical glucose sensors sometimes need labels as in the case of fluorescence-based sensors. Commonly-used fluorescent markers, based on organic dyes [15,16,69] and semiconductor quantum dots [18, 47, 75], can exhibit photobleaching and toxicity effects. Optical spectroscopic techniques have also been developed, at the cost of being more expensive and difficult to miniaturize [3]. In comparison, non-enzymatic electrochemical glucose sensors offer simpler operation, ease of miniaturization and scalability, lower cost, and portability.

Most electrochemical non-enzymatic glucose sensors are based on precious noble metals and their alloys (e.g. Pt, Au, Pd, and Rh) [2, 52, 53, 66], transition metals (e.g. Cu, Ni, Zn, and Mn) [81,84], metal-oxide (e.g. NiO and CuO) [57,88], semiconductor nanostructures (e.g. graphene and MoS2) [23, 63], and their combination for viable alternatives to traditional enzymatic sensors. [25,63,84] Among various catalytic materials for oxidation of glucose, Ni and Cu compounds are promising due to their low cost, good electrochemical stability, and high electrocatalytic properties. [1, 5, 24, 42, 43, 56, 68, 85] For example, decorating Ni nanoparticles (NPs) on glassy carbon electrodes modified with carbon nanotubes exhibited good electrocatalytic activity with a 10 nM detection limit and a wide linear range (0.25 – 1200 μM) toward the electro-oxidation of glucose in alkaline NaOH solution. [19] In another work, it was shown that a Cu electrode modified with Ni NPs and multiwalled carbon nanotubes can achieve a 2 μM – 10 mM linear range in alkaline environment. [86] Recent reports of nickel-oxide (NiO) electrodes have also shown a good response for glucose with an advantage of being more stable compared to Ni. [5, 25, 27] It was shown that NiO electrodes can enable detection of glucose in the concentration range of 0.005 mM – 5.5 mM in NaOH (pH 13). [27] Ni was first electrodeposited onto nickel foam, followed by annealing at 300°C for 3 hours to fully transform α-Ni$(OH)_2$ to NiO. [27] Nafion-coated Cu nanowires synthesized using a wet-chemistry – using $Cu(NO3)_2$, concentrated NaOH, EDA, and N_2H_4 – enabled detecting glucose as low as 35 nM in NaOH (pH 13) with a linear response up to 3 mM. [43] In another work, Cu-Ni modified pencil graphite was used for detection of glucose. Cu was electrodeposited using cyclic voltammetry (CV) onto a pencil lead in an acidic solution containing copper sulfate (pH 3.5) [50], followed by Ni electrodeposition in a solution containing nickel sulfate (pH 6.5). [12] The electrode showed a limit of

detection of 1 nM and a linear range to 10 mM in NaOH (pH 13). [50]

However, as highlighted above, non-enzymatic and non-noble metal-based catalytic electrodes for glucose oxidation operate in highly-alkaline media which can be challenging for real-world applications, damage electrode materials, and impose storage/operation hazards. [3, 56]10,30–34 In this work, we introduce a low-cost and scalable method to synthesize a non-noble metal catalyst for detection of glucose in non-buffered near-neutral solution of sodium sulfate as the background medium (pH 6.4). The sensing electrodes are created using sequential electrodeposition of Cu nanostructures on Ni followed by an optimized two-step annealing process and electrochemical treatment/stabilization in phosphate buffer saline (PBS). The electrochemical sensors using PBS-Cu-Ni as working electrode achieve a high sensitivity with a low detection limit of 1 nM, a dynamic range up to 20 mM, and an applied potential of 0.2 V. The effect of sequential electrodeposition, annealing, and PBS stabilization on surface morphology and elemental composition are studied using Scanning Electron Microscopy (SEM) and Energy Dispersive X-Ray Spectroscopy (EDS). Moreover, the sensor enables an excellent selectivity toward glucose compared to ascorbic acid, dopamine, and uric acid. Not only is the PBS treatment critical for the enhanced sensitivity of PBS-Cu-Ni electrodes (by 60% compared to Cu-Ni electrodes), it improves the sensor stability (average signal change of only 8% vs. 35% after one week storage in ambient condition). The simple and scalable fabrication of the sensing electrode using electrodeposition and its good selectivity can provide a promising route for development of inexpensive non-enzymatic, disposable glucose sensors for in vitro testing at the point-of-care.

2.2 Experimental procedure and Results

2.2.1 Electrodeposition of nickel (Ni)

Glass slides were first cleaned in piranha solution (4:1 – H_2SO_4:H_2O_2) for 30 minutes to remove any organic residues. This is followed by an electron-beam (e-beam) deposition of a seed layer of Cr/Au (10 nm/100 nm). Ni is then electrodeposited in High Speed Nickel Sulfamate Plating Solution using a two-electrode configuration, comprised of a stainless-steel reference/counter electrode. Ni with about 10 mm thickness is deposited using chronopotentiometry with a current density of -6 mA/cm^2 for 125 minutes. A PalmSens4 potentiostat and PSTrace5 software are used to control the deposition process. The electrode set up can be seen in Fig. 2.1. The resulting potential curve from the

deposition can be seen in Fig. 2.2a.

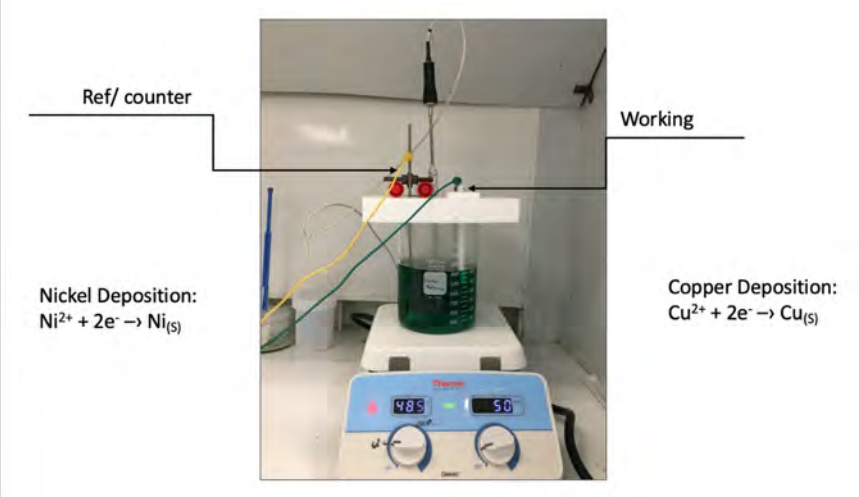

Figure 2.1. Electrodeposition set up. The reference (ref.)/counter electrode was a stainless steal plate, working electrode was a 1 cm by 1 cm Cr/Au sample.

2.2.2 Electrodeposition of copper (Cu)

After rinsing the substrate with DI water, Cu is electrodeposited via chronopotentiometry at a current density of -3 mA/cm^2 for 2 minutes (in the same setup used for Ni deposition). The deposition solution consists of 5 mM of $CuSO_4$ as the Cu source mixed in 50 mM of Na_2SO_4 as the background electrolyte (pH 6.4). A PalmSens4 potentiostat and PSTrace5 software are used to control the deposition process. The electrode set up was the same as the Ni electrodeposition, as seen in Fig. 2.1. The resulting potential curves from the depositions is shown in Fig. 2.2b.

2.2.3 Electrochemical characterization

Electrochemical characterization is carried out using cyclic voltammetry (CV). A three-electrode configuration with a platinum counter electrode (Basi, Co.), Ag/AgCl reference electrode (Basi, Co.), and the developed electrodes as the working electrode are employed. The electrochemical measurement setup is contained in an electrical probe station. For CV measurements, the potential is swept at different scan rates from 10 mV/s to 500 mV/s over a range of -0.6 V to 0.35 V.

To prepare the samples for testing the sensors, glucose powder is dissolved in a solution of 100 mM Na2SO4 in DI water at concentrations from 1 nM to 20 mM. CV

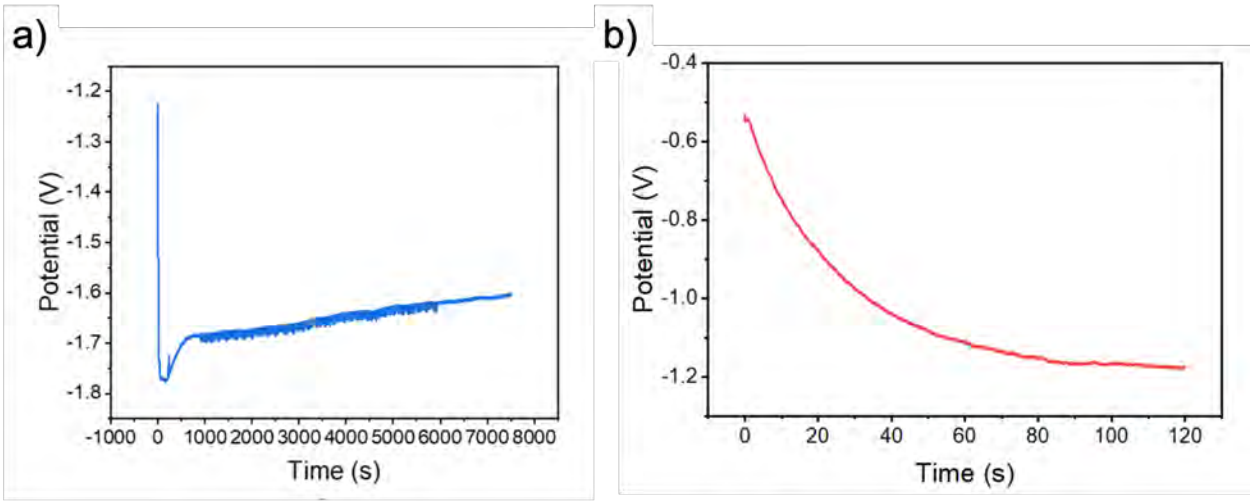

Figure 2.2. Electrodeposition curves a) the potential curve during the Ni deposition b) the potential curve during the Cu deposition.

measurements are used to evaluate the response to different glucose concentrations as well as interfering analytes. Each CV cycle consists of a reduction direction from 0.35 to -0.6 V, followed by oxidation in the opposite direction. CV scan rate of 50 mV/s is used for analytical testing. In all electrochemical measurements, polyimide tape was used to isolate the active electrode area from the contact pads and electrical probes.

2.2.4 Sensor Development and Characterization

Figure 2.3 demonstrates the process for synthesis of PBS-Cu-Ni electrodes. The Cu-Ni samples are prepared as described in Section 2.2.1 and Section 2.2.2. After storing the sample in ambient conditions for four days (Step 1), the Cu-Ni electrode is further annealed at 150°C for 1 hour (Step 2). Various annealing conditions were explored (summarized as T1, T2, T2P, and T3 in the Appendix A) and showed that the initial long-term ambient annealing is required to achieve high sensitivity. We believe this step creates stable phases of copper oxide which is shown to demonstrate good catalytic properties for oxidation of glucose. [68] After the two-step annealing process, we create PBS-Cu-Ni electrodes by performing cyclic voltammetry (CV) in PBS until successive CV curves overlap which marks electrode stabilization. PBS treatment not only enhances the sensor sensitivity toward glucose (as seen in Appendix A), but also significantly improves its stability discussed in Section 2.2.5.

We studied the effect of annealing and PBS treatment on surface morphology. Comparing the scanning electron microscope (SEM) images in Figure 2.4 a and b suggest

that annealing results in growth of Cu crystal nucleation sites as well as improving the surface uniformity. After electrochemical stabilization/treatment in PBS, the surface morphology undergoes further changes – crystal growth and formation of additional nanostructures on top of the Cu microcrystals – as shown in Figure 2.4 c.

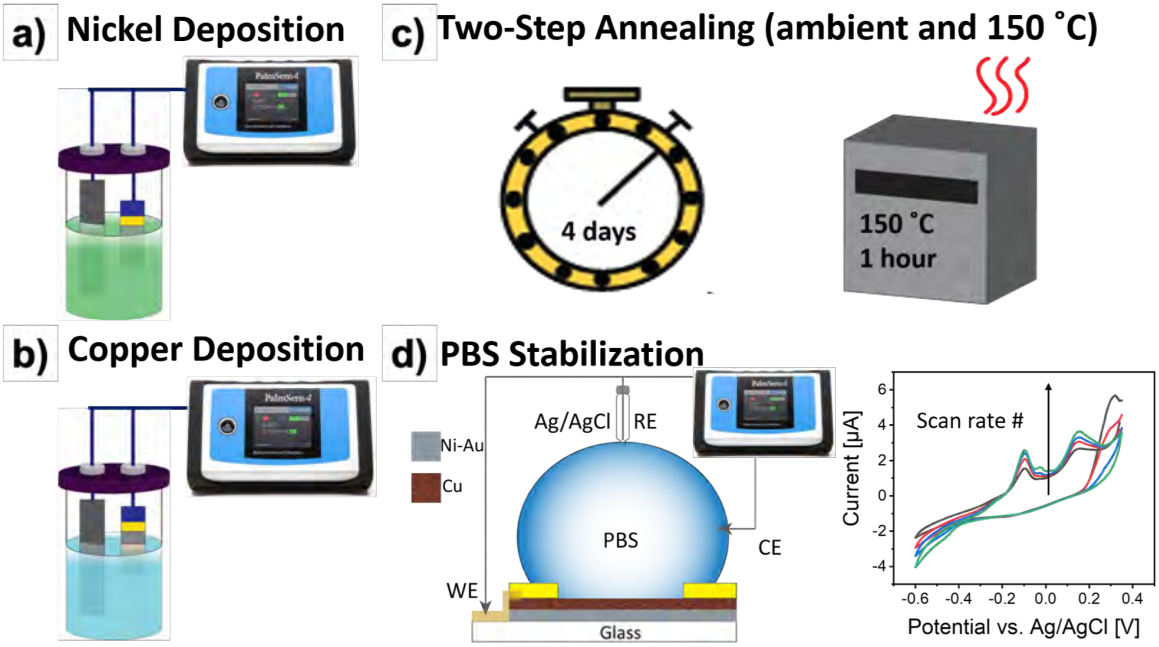

Figure 2.3. Fabrication schematic a) Electrodeposition of nickel (Ni) on thin film gold (Au) layer deposited on glass substrate. b) Copper (Cu) electrodeposition at 50°C for 2 min. c) The two-step annealing process, with Step 1 in air at room-temperature for four days, followed by Step 2 at 150°C for 1 hour. d) Electrochemical treatment of Cu-Ni electrodes in PBS using cyclic voltammetry (CV). At least 45 scans are performed until CV curves are stabilized. The inset shows representative CV curves.

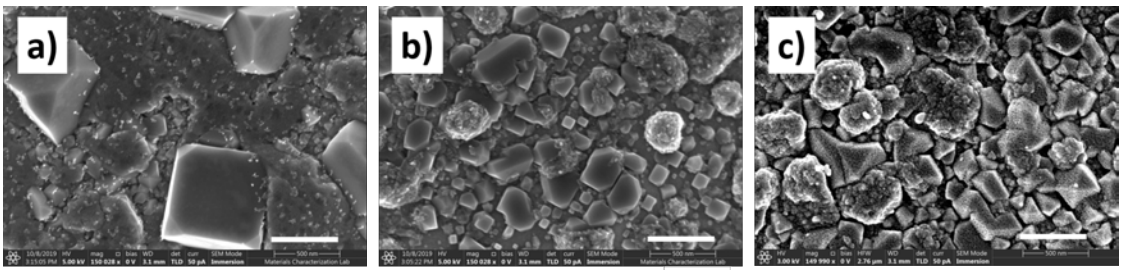

Figure 2.4. SEM imgaes of a) Cu-Ni electrode before the two-step annealing process, b) Cu-Ni electrode after the two-step annealing, c) PBS-treated Cu-Ni (PBS-Cu-Ni) electrode. Scale bar: 500 nm.

Figure 2.5 a-c depict the EDS maps for chlorine, copper, phosphate, and oxygen respectively in a PBS-Cu-Ni electrode. Figure 2.5c demonstrate the corresponding

SEM image indicating formation of nanostructures. The nanostructures in PBS-Cu-Ni electrodes enhance sensing capability by providing a high surface area and more active sites to facilitate the electro-catalysis of glucose. Increase of active sites results in improved sensing. [73] Interestingly, similar flower-like nanostructures of $Cu_3(PO_4)_2$ were reported to form spontaneously by exposing copper to PBS, which resulted in improved protein functionalization by He et al. [30] The EDS maps in Figure 2.5 indicate that after nanostructure formation, the presence of Cl on the copper surface is similar (ca. 0.37 wt%) to the previously reported value (ca. 0.2 wt%), [30] where the authors showed that the Cl^- ions in PBS are indispensable for the formation of the nanoflowers. It was observed that the flower-like structures did not form if Cl^- was not present in the solution during material synthesis. [30] Hence, we also speculate that the formation of the nanostructures is caused by dissolved oxygen, Cl^-, and $PO4^{3-}$. [30] In the presence of Cl^- ions, Cu is oxidized by the dissolved oxygen and forms CuCl, which in turn converts to $CuCl^{2-}$, followed by dissolving with phosphate to form $Cu_3(PO_4)_2$. Another possibility is formation of Cu_2O via hydrolysis ($2CuCl + 2OH^- \rightarrow 2Cl^- + Cu_2O + H_2O$). [30] The detailed EDS analysis of elemental composition for Cu-Ni electrode before and after annealing and after PBS treatment is provided in Table 2.1.

Element	At %		
	Cu-Ni	Cu-Ni (Annealed)	PBS-Cu-Ni
Ni	51.8	46.3	48.1
Cu	35.1	37.4	27.1
C	8.7	12.1	15.6
O	3.6	4.4	5.9
Cl	0.3	0.1	0.6
P	0	0	1.6
S	0.1	0	1.3
Si	0.4	0	0

Table 2.1. EDS data comparing the elemental composition of different steps of fabrication.

In addition to material characterization, we evaluated the electro-catalytic activity of electrodes before and after deposition of Cu, and after PBS treatment using CV measurements over a range of -0.6 V to +0.35 V vs. Ag/AgCl reference electrode. Figure 2.2.3 a displays the cyclic voltammograms of the PBS-Cu-Ni, Cu-Ni, and Ni electrodes in 0.1 M Na_2SO_4 in the presence of 5 mM glucose at a scan rate of 50 mVs^{-1}. These results confirm that deposition of Cu improves the catalytic response (anodic current) compared to bare Ni by 600% at the sensing potential of 0.2 V, noting that bare Ni is not catalyzing glucose oxidation as there is no Faradaic peak in the CV curve. Importantly,

PBS treatment of the Cu-Ni electrodes to form PBS-Cu-Ni results in an additional improvement by 120%. Figure 2.6 b shows the CV of PBS-Cu-Ni electrodes recorded in 0.1 M Na_2SO_4 solution at different scan rates in the range of 10 – 500 mVs^{-1}. It is found that the anodic and cathodic peak currents are linearly correlated to the square root of the scan rate with a linear regression of I_{pa} (µA)= 0.32479x-0.07685 (R=0.993) and I_{pc} (µA)= -0.1179x-0.39673 (R=0.996), respectively. These results indicate that the glucose redox reaction is semi-reversible and mostly a diffusion-controlled process. [44]

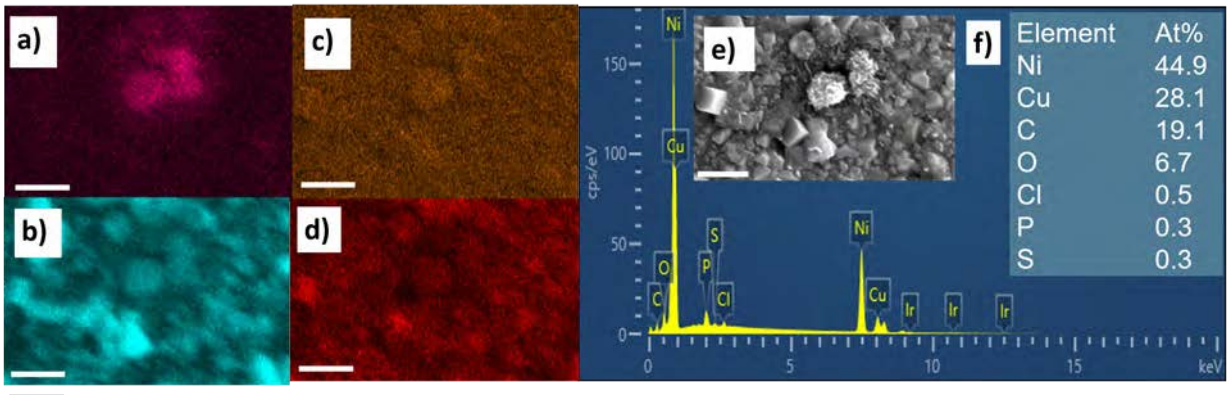

Figure 2.5. Morphology and elemental composition of PBS-Cu-Ni electrode. EDS maps for a) chlorine (Cl), b) copper (Cu), c) phosphorous (P), d) oxygen (O). e) The corresponding SEM image. f) Atomic percentage (AT%) for the elemental composition of PBS-Cu-Ni. Scale bar: 5 µm.

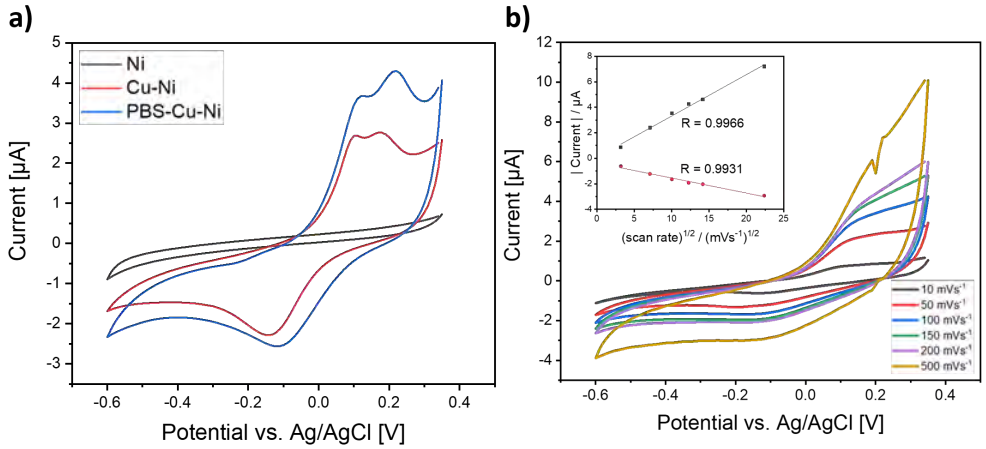

Figure 2.6. Cyclic voltammogram (CV) curves of a) 5 mM glucose in 0.1 M Na_2SO_4 for Ni, Cu-Ni, and PBS-Cu-Ni electrodes. b) CV curves at different scan rates from 10 to 500 mVs^{-1} of 1 mM Glucose in 0.1 M Na2SO4. The inset shows the relationship between the oxidation (black curve) and reduction (red curve) peak current vs. the square root of the scan rate.

2.2.5 Sensor performance: sensitivity, selectivity, and stability

As previously discussed in the Section 2.1, Cu and Ni have been utilized in developing non-enzymatic sensors for detection of glucose oxidation. [11, 38, 40, 81] However, much of the prior reports require operating in highly-alkaline solutions, or require at least 0.5 or 0.6 V to achieve large signal to noise. In contrast, our results using PBS-treated Cu-Ni electrodes (Figure 5a) show that glucose can be detected reliably in an outstanding wide range from 1 nM to 20 mM in near- neutral pH of 6.4 using only about 0.2 V vs. Ag/AgCl. The ultralow detection limit is a result of synergistic activity of Cu, $Cu_3(PO_4)_2$, and Cu_2O which is formed due to CV treatment in PBS and reduction of CuO to from Cu_2O. The synergistic behavior results in 120% improved CV current at the sensing potential (0.2 V) with PBS-Cu-Ni vs. Cu-Ni electrode – as well as the nanostructured surface of PBS-Cu-Ni electrodes which lead to enhanced sensitivity compared to Cu-Ni.

The rough mechanism for oxidation of glucose at PBS-Cu-Ni electrode is speculated to be the following: $Cu_3(PO_4)_2$ or Cu_2O will electrochemically oxidize to Cu(III) species such as CuOOH or $Cu(OH)_4$. Next, glucose is oxidized by Cu(III) to form hydrolyzate gluconic acid, i.e. Cu(III) + glucose $\rightarrow$ gluconolactone + Cu(II), followed by gluconolactone $\rightarrow$ gluconic acid via hydrolysis. [50] We believe that electro-oxidation of glucose to glucolactone is also catalyzed by the Ni(II)/Ni(III) redox couple, [50] although the dominant contribution is through copper redox reactions as evident from significantly smaller Faradaic current with bare Ni electrode vs. Cu-Ni (Figure 2.2.3 a).

In addition to high sensitivity and low detection limit, a good sensor should also be selective toward the target analyte. A main challenge of non-enzymatic glucose sensors is the interference of other substances in the blood besides glucose, which can be oxidized at potentials comparable to glucose. Biomolecules, including ascorbic acid (AA) and uric acid (UA) often co-exist with glucose in human physiological fluids, and hence are important interferences to consider in electrochemical oxidation of glucose. In physiological samples of saliva, glucose concentration is generally 65 µM, UA is 175.4 µM and AA is 600 nM. [28, 54, 65] As such, to study the sensor selectivity, we tested PBS-Cu-Ni sensors with diluted physiological levels glucose, UA, and AA in artificial saliva. Two dilutions of the physiological levels of artificial saliva into Na_2SO_4 were tested: 1% and 3%. The CV curves in Figure 2.7b inset are almost identical with and without the interfering molecules, confirming excellent selectivity of PBS-Cu-Ni electrodes for oxidation of glucose.

The long-term stability is another important factor when comparing different sensors. We measured the response of Cu-Ni and PBS-Cu-Ni after one week with different

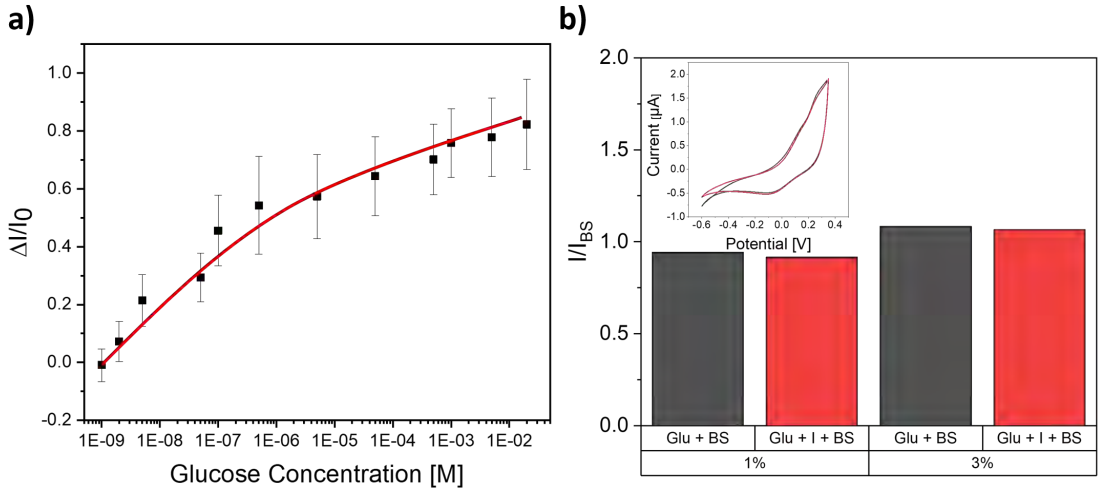

Figure 2.7. Sensor sensitivity and selectivity. Cyclic voltammograms (CV) curves of a) peak oxidation current at 0.2 V normalized by the baseline current, I_0, for various glucose concentrations in 0.1 M Na2SO4 (pH 6.4). The error bars depict the standard errors with n = 3. CV curves for b) 1% and 3% diluted artificial saliva with 65 µM, UA is 175.4 µM and AA is 600 nM into Na_2SO_4 normalized to the baseline of artificial saliva and Na_2SO_4.

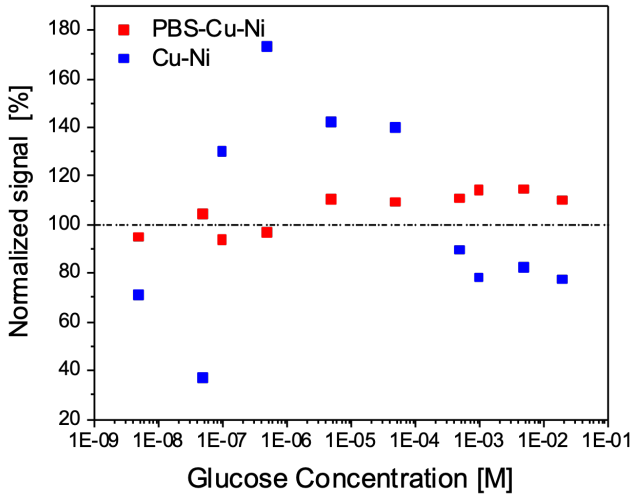

Figure 2.8. PBS treatment is essential for sensor stability. The oxidation current on day seven normalized to the initial signal (on day one) over the entire sensor dynamic range (5 nM- 20 mM). The sample was stored in ambient condition.

concentrations of glucose in 0.1 M Na_2SO_4. The normalized signals (oxidation current values) with respect to the first day are plotted in Figure 2.7, suggesting only 8% change on average (less than 15% change in individual days) through the course of one week for the PBS-Cu-Ni sensors. This result confirms that PBS stabilization enhances the sensor stability over time. On the other hand, the Cu-Ni samples are significantly less stable

with an average change of 35% between the initial day and the seventh day, with values fluctuating between 20%- 180%.

Table 2.2 provides a comparison between some of the reported non-enzymatic glucose sensors with our work. Except a few works which utilize noble metals (such as Au and Pt) [2,3,66], almost all reported non-enzymatic glucose sensors require alkaline pH which impose challenges for safe storage as well as damaging the sensor electrodes and hence reducing the sensor life time.

Material	Dynamic Range	Limit of Detection	Applied Potential	Medium pH	Medium	Ref
Ni NPs on GCE modified with CNTs	0.1 – 5000 µM	2 nM	0.4 V	13	NaOH	[19]
Cu electrode modified with Ni NPs and MWCNTs	2 µM - 10 mM	0.7 µM	0.35 V	13	NaOH	[86]
NiO	0.005 – 5.5 mM	5 µM	0.47 V	13	NaOH	[27]
Cu NWs	35 nM – 3 mM	35 nM	0.6 V	13	NaOH	[84]
Ni-Cu/PGE	1 nM – 10 mM	1 nM	0.5 V	13	NaOH	[50]
Cu/MWCNT	0.7 µM – 3.5 mM	0.21 µM	0.65 V	12	NaOH	[34]
Cu/SWCNT/ GCE	0.5 – 100 µM	0.25 µM	0.65 V	12.7	NaOH	[45]
Ni-Cu/TiO_2 NTs	10 µM - 3.2 mM	5 µM	0.6 V	13	NaOH	[38]
CuxO/PPy/ Au	6.2 µM – 8 mM	6.2 µM	0.6 V	13	NaOH	[48]
Pt/CuO/Pt	2.2 mM – 10 mM	2.2 mM	1 V	7	H_2O	[2]
Au@Pt NPs	0.5 – 10.0 µM 0.01 – 10 mM	445 nM	0.1 V 0.35 V	7.4	PBS	[66]
PBS-Cu-Ni	5 nM – 20 mM	1 nM	0.2 V	6.4	Na_2SO_4	This work

Table 2.2. Comparable glucose sensors are listed displaying various characteristics of each sensor. NPs: nanoparticles, CNTs: carbon nanotubes, GCE: glassy carbon electrode, MWCNTs: multi-walled carbon nanotubes, PGE: Pencil graphene electrode, SWCNT: single-walled carbon nanotube, PPy: polypyrrole.

2.3 Conclusion

This work demonstrates synthesis and application of PBS-treated Cu-Ni electrodes as the working electrode for non-enzymatic electrochemical sensing of glucose in near-neutral pH which is a distinct advantage compared to other non-noble metal glucose catalysts. PBS-Cu-Ni electrodes show excellent selectivity for detecting glucose in the presence of physiological levels of uric acid and ascorbic acid in artificial saliva. Cyclic voltammetry analysis showed an ultralow limit of detection of 1 nM with a wide dynamic response in the range of 5 nM – 20 mM. In addition to enhancing the sensor sensitivity by 120%, the PBS treatment is essential for stable operation in the entire dynamic concentration range. With further material optimization, the proposed all-electrochemically synthesized PBS-treated Cu-Ni structures may offer the ability to directly measure glucose in biologically complex media, such as blood.

Chapter 3
Developing Hydrogen Peroxide Sensors using Laser Written Platinum Electrodes

This chapter discusses the use of laser written platinum (LW-Pt). In Section 3.1 the importance hydrogen peroxide detection is discussed. Then the fabrication process, characterization, experimental procedure, and results are explained in Section 3.2. Finally in Section 3.3, the experimental findings are summarized. The laser-written samples were provided by Alex Castonguay in Dr. Lauren Zarzar's group at PSU through a funding provided by the Materials Research Institute's Humanitarian Award.

3.1 Introduction

Hydrogen peroxide (H_2O_2) is very important in various fields including environmental safety, clinical, and biological systems. [87] H_2O_2 is also a stable reactive oxygen species (ROS). [20, 87] H_2O_2 is a by-product in almost all oxidase activities. [20, 79] Enzymes such as glucose oxidase (GOD), cholesterol oxidase (ChoOx), glutamate oxidase (GlOx), oxalate oxidase (OxaOx), and lactate oxidase (LOx) all produce H_2O_2 as a by-product when used as a catalyst. [20,78] As such, detection of H_2O_2 can be used as a quantitative way to measure the activity of certain enzymes and an indirect way to measure the amount of a target analyte such as glucose or lactic acid. [61]

A popular method of detecting H_2O_2 is by the use of enzymes. The most common enzyme used is horse-radish peroxidase. [33,51] Enzymatic methods fall into two categories: mediator free and mediator-based sensors. [20] However, as mentioned in Section 2.1 enzymes have some limitations. Non-enzymatic sensors are also not limited by the

presence of oxygen as some enzyme-based methods are. [20] Metals such as platinum (Pt), gold, silver, palladium, nickel, and copper are frequently used as catalysts for detection of H_2O_2. [20, 35, 62] Among them, Pt is of particular interest because of its selectivity to H_2O_2. [13]

Pt nanoparticles have been used to detect H_2O_2 as they have high electrocatalytic efficiency with large surface to volume ratio. [7, 13] Recent Pt-based non-enzymatic H_2O_2 senors focus on modified Pt nanoparticles. Platinum nanoparticles (PtNPs) on a glassy carbon electrode (GCE) is one example. [31] In this work, GCE was polished and then poly-melamine was electro-polymerized on GCE. Finally PtNPs were deposited onto the electrode. This method had a limit of detection of 650 nM in PBS. Another example is Pt NPs that were fabricated using a plant-based extract. The extract of the plant *Nymphaea alba* was used as the reducing agent for a platinum chloride solution to create PtNPs. These PtNPs were added to a carbon paste to create electrodes. This method achieved detection of 700 nM in a phosphate buffer solution (pH 5). [49]

In this work, the laser-written Pt (LW-Pt) fabricated using a laser-writing technique was characterized using SEM and XPS. The electrochemical behavior was studied using CV and SWV methods. The effect of background medium, salt concentrations and SWV frequency were studied. The sample lifetime, sensitivity, and selectivity were studied. The limit of detection was found to to be 5 fM of H_2O_2 in PBS (pH 7.2) without the use of enzymes.

3.2 Experimental Procedure and Results

3.2.1 Materials and Methods

3.2.1.1 Laser Writing Method

The LWM-Pt was fabricated by covering an area of a glass slide with $(NH_4)_2PtCl_4$ in water. Borosilicate or conductive Fluorine doped Tin Oxide (FTO) (Sigma Aldrich, Co.) covered glass was used as the substrate to the Pt. Then a Titanium:Sapphire laser of about 780 nm wavelength (MIRA 900-F) (Coherent, co.) with a 40x objective (Nikon, Co.) was applied continuously. This creates a Thermal Voxel where very high temperatures are reached (possibly up to 2000 K). The heat causes localized thermal decomposition, resulting in the formation of nanoparticles whose crystal structure depends on the precursor salt and solvent used. The fabrication process can be seen schematically in Fig. 3.1. The details of the deposition can be found in Ref. [82].

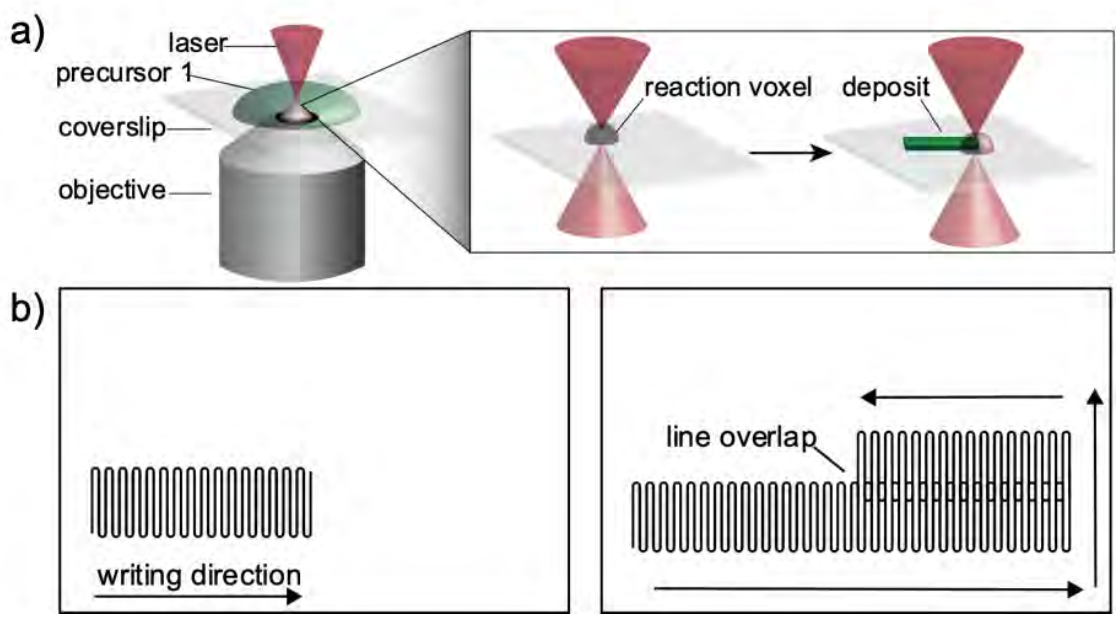

Figure 3.1. Fabrication steps to create laser-written metals. a) The laser writing setup, b) the laser writing pattern. These figures are provided by Alex Castonguay.

3.2.1.2 Material Characterization

The SEM images of the Pt samples, shown in Fig. 3.2, indicate that the material is very porous with nano-meter pores. This leads to a very large active area available for sensing. The large active area contributes to the high sensitivity since there are more active sites for the redox reaction to take place.

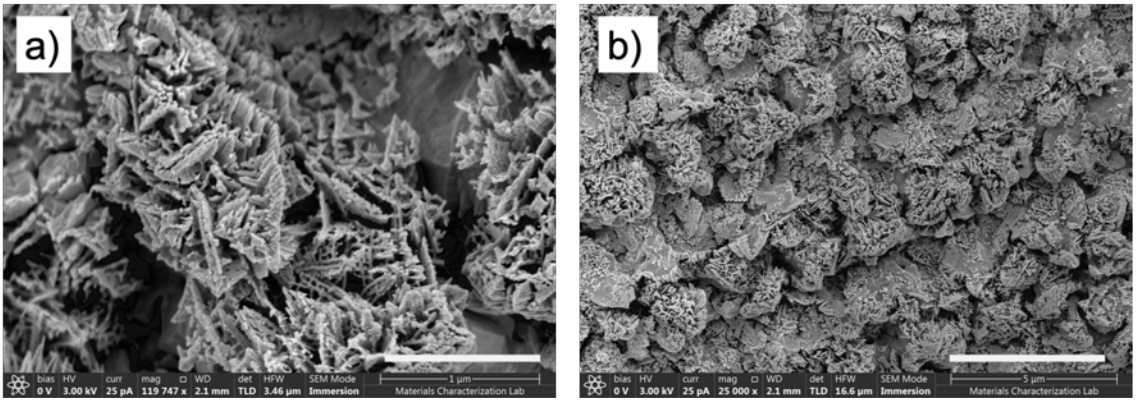

Figure 3.2. SEM images of LW Pt samples a) scale bar 1 µm, b) scale bar 5 µm. These figures are provided by Alex Castonguay.

XPS was used to confirm the presence and phase of Pt.There is a peak around 71 binding energy that confirms the presence of metallic Pt. XPS was performed using

Physical Electronics VersaProbe II.

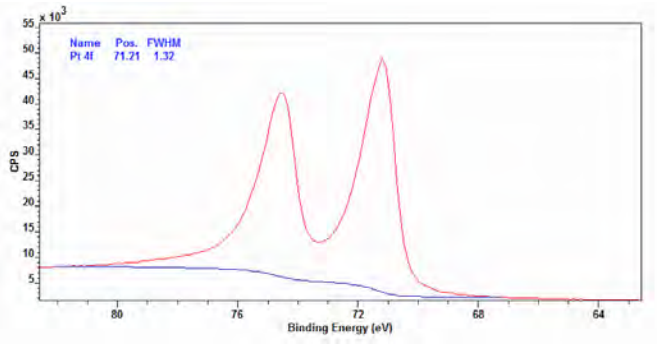

Figure 3.3. XPS of LW Pt samples. This data is provided by Alex Castonguay.

3.2.1.3 Electrochemical Testing Method

Electrochemical characterization with various concentration of H_2O_2 in 100 mM KCl (Sigma Aldrich, co) or PBS (pH 7.2) (VWR, co.) is carried out using CV and SWV. A three-electrode configuration with a platinum counter electrode, Ag/AgCl reference electrode, and the developed electrodes as the working electrode are employed as seen in Fig. 3.4. The electrochemical measurement setup is contained in an electrical probe station. For CV measurements, the potential is swept at a scan rate of 50 mV/s (unless stated otherwise) over a range of -0.5 V to 0.5 V. SWV scans had a wait time of 30 seconds, amplitude of 25 mV, swept from -0.25 V to 0.25 V, and a frequency of 3 Hz. Fig. 3.5 a and b show representative SWV and CV data obtained using a sensor made with 0.25 salt concentration on FTO-glass. The frequency of 3 Hz was chosen as the testing frequency because the signal has the largest slope or highest sensitivity at this frequency. To identify the optimum working frequency, we tested samples with different exposed area. Our results in Fig. 3.7b show that for a testing area of a circle with 2 mm diameter, the optimum frequency is 3 Hz. The optimum frequency for sensors with different exposed area should be identified first to ensure the highest sensitivity possible.

3.2.2 Characterizing laser-written Pt working electrodes for sensing H_2O_2

3.2.2.1 Studying the effect of salt concentration on sensitivity

We studied the effect of the different precursor salt (solution of $(NH4)_2PtCl_4$ in water) concentrations and size of the printed sample with respect to H_2O_2 response. The sensor

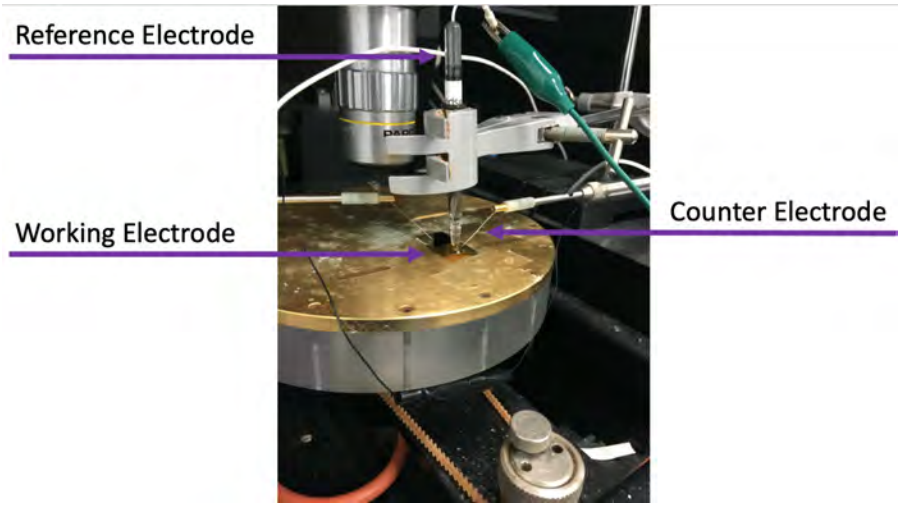

Figure 3.4. The testing setup with Pt CE, Ag/AgCl reference electrode, and LW-Pt as the WE.

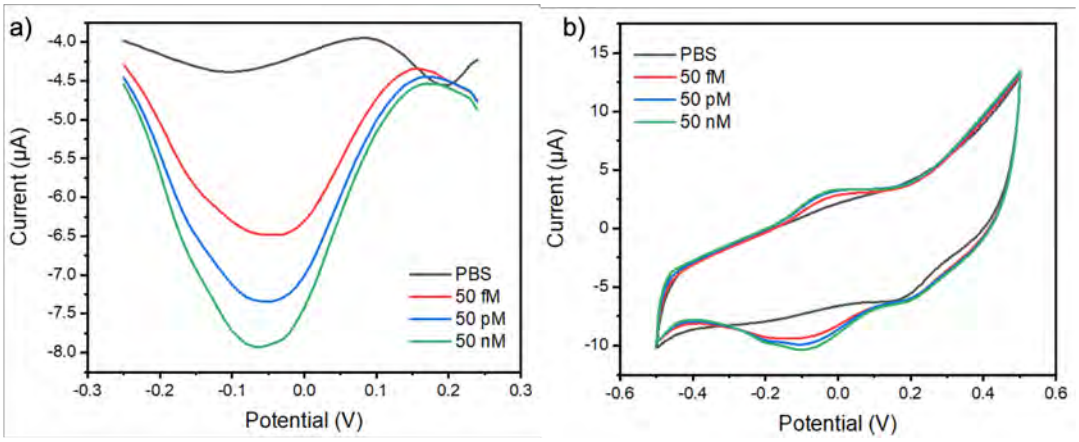

Figure 3.5. The current-voltage curves obtained with various concentrations of H_2O_2 in PBS using a) SWV, b) CV. SWV yields a higher sensitivity and the analytical method of choice in this work..

response at different peroxide concentrations is plotted in Fig. 3.6. Δ I is defined as I - I_0, where I is obtained from SWV data at 3 Hz, and I_0 is the response during a scan of only the media (in this case PBS). The slope of this curve corresponds to the sensor sensitivity. In Fig. 3.6a, the sensor sensitivity in the case of electrodes printed on FTO substrate decreases with the decrease of the concentration of salt during the writing process. This is expected, as less salt means less Pt being printed which results in less available sensing material on the working electrode. Even though 0.5 M salt has the highest sensitivity, we choose to focus 0.25 M salt concentration to conserve the salt as it is expensive.

3.2.2.2 Studying the effects of substrate and precursor salt concentration on sensitivity

The material on FTO glass was very promising as discussed in Section 3.2.2.1. However, for an on-chip sensor that has all the electrodes printed onto one substrate, the substrate needs to be non-conductive. As such, the samples were fabricated with 0.25 M salt concentration on non-FTO glass (borosilicate glass). The sensitivity of the non-FTO glass is 0.244 times higher than the FTO sample with the same salt concentration, as seen in Fig. 3.6. This is promising for on-chip sensors where the dielectric nature of non-FTO will allow writing all the electrodes (working, counter, and reference electrodes) on the same substrate. We observed larger standard error for the non-FTO glass in comparison with the FTO glass. The larger error may be from misalignment from of the laser. This misalignment may cause unpredictable thickness variation of samples.

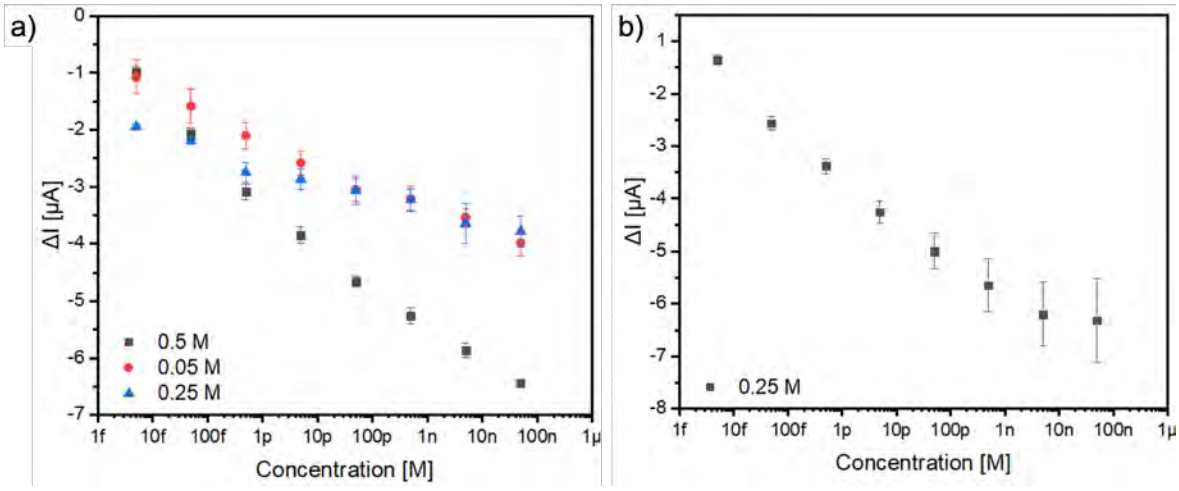

Figure 3.6. The effect of the precursor salt concentration and FTO vs. non-FTO substrates. a) response to H_2O_2 in PBS printed using precursors with different salt concentrations on FTO glass (0.5 M slope = -0.73, 0.05 M slope = -0.39, 0.25 slope = -0.27), b) response to H_2O_2 using PBS in 0.25 M salt on non-FTO glass (slope = -0.66).

3.2.2.3 Studying the effects of background medium and SWV frequency on sensitivity

The effect of background medium was explored. The background solution of electrochemical tests needs to be conductive to help facilitate the redox reactions. So, the first background investigated was 100 mM KCl in DI water. Since the KCl is a simple salt solution, we explored if the LW-Pt still responded to H_2O_2 in a more complex solution

and biologically relevant background. As such, the buffer solution, PBS, was used as the alternative background. Fig. 3.7a shows the response to various concentrations of H_2O_2 in both 100 mM KCl and PBS on 0.5 M Pt salt concentration, at 3 Hz frequency. There does not seem to be a large difference between the KCl and PBS background. We chose to conduct all further testing in PBS.

Fig. 3.7b shows the response of the of samples of different sizes (small = 123.4 x 104.9 µm, medium = 1.042 x 0.997 mm , normal = 2 mm diameter circle) and different frequencies using SWV data with 0, 50 fM, 50 pM, 50 nM H_2O_2 in PBS. As noticed, generally, the larger the exposed sample area, a lower frequency is needed to optimize the response of H_2O_2 in PBS.

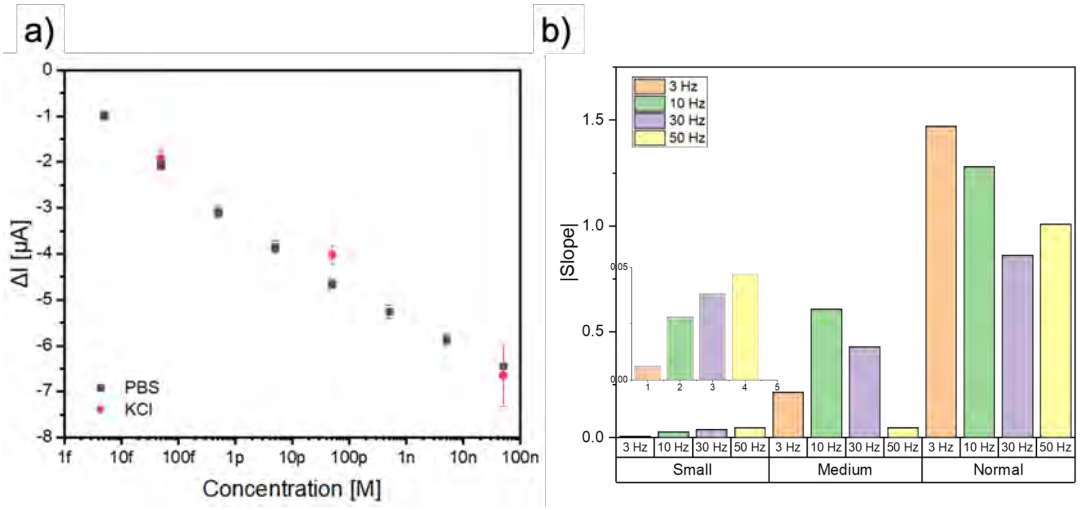

Figure 3.7. The effect of different background solutions and SWV frequency. a) various concentrations of H_2O_2 in PBS or 100 mM KCl were studied, b) the slope (sensitivity) of sensors with different exposed The inset shows the magnified view of the area. signal using "Small" sensor surface area.

3.2.2.4 Studying the lifetime and effects of dissolved oxygen

The re-usability and lifetime of samples were studied. When initial lifetime studies were conducted, we noticed that there was a change in the shape (or shift) of the baseline between different days as seen in Fig. 3.8a. Lifetime tests were conducted by testing the same sample with PBS and then 5 nM of H_2O_2 at 3 Hz sweeping the voltages as discussed in Section 3.2.1.3. From Day 1 Bl (baseline/background) to Day 3 Bl (baseline/background) a peak around -0.1 V was created even though there was no H_2O_2 present in the PBS. This prompted the study of multiple testing trials during the same day. Trial 1 through 3 consisted of PBS rinsing and H_2O_2 testing in PBS. Trial 4

consisted of 99% IPA rinsing, PBS rinsing, then H_2O_2 testing in PBS. The stabilized PBS baseline seemed to increase current magnitude between Trials 1-3 as seen in Fig. 3.9a. It was noticed, however, that the baseline did decrease in magnitude after the IPA rinsing. Though when looking at the overall ΔI response of the sample, the sensitivity (slope) decreases over the trials making Trial 4 have the lowest sensitivity shown in Fig. 3.9b. From these resutls we conclude that the samples are suitable for single-use and disposable sensing applications.

We also studied the affect of dissolved oxygen on the sensor response for detection of hydrogen peroxide. As Pt is a good catalyst for hydrogen evolution reaction (HER), it was necessary to check if the sensor responds to hydrogen peroxide in nitrogen-purged solution. [14, 64] As seen in Fig. 3.8, the samples are still responsive to H_2O_2 down to 5 fM, although the sensitivity (slope of the curves) is slightly less compered to the results in the presence of oxygen.

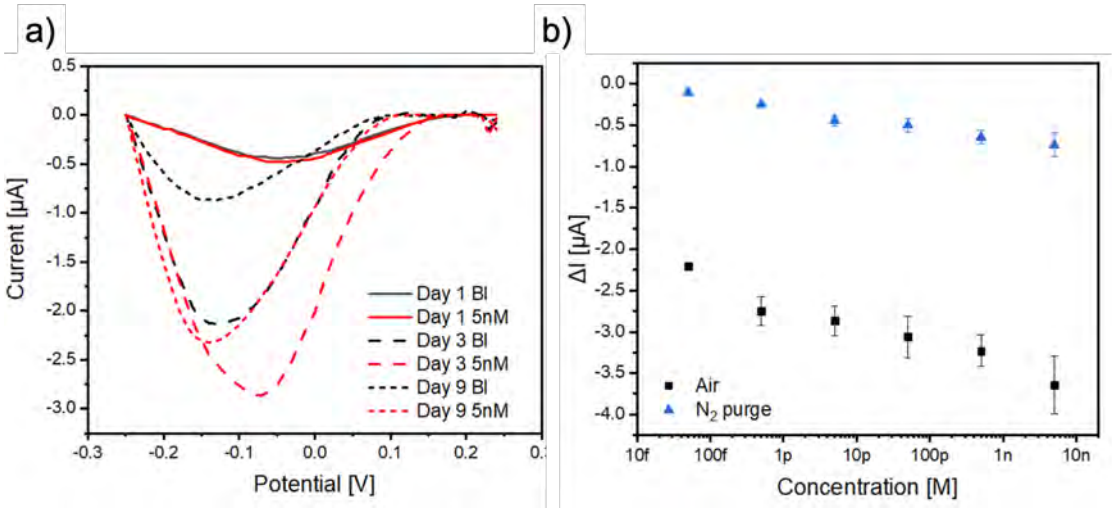

Figure 3.8. Sensor lifetime and effect of dissolved oxygen. a) The SWV response of the same sample over multiple days tested with PBS and PBS with 5 nM H_2O_2 at 3 Hz b)the response to H_2O_2 N_2-purged to remove all dissolved O_2 in the solution on FTO glass as the substrate.

3.2.2.5 Studying the effect of interfering analytes

Similar to Section 2.2.5, testing the selectivity of the material to other electro-active analytes is necessary. These tests were conducted in PBS using the same three-electrode set up as the other tests. Samples were fabricated on borosilicate glass with no FTO covering. The samples were fabricated using 0.25 M Pt salt concentration. Common interfering molecules for H_2O_2 are uric acid (UA) and ascorbic acid (AA). [13] These

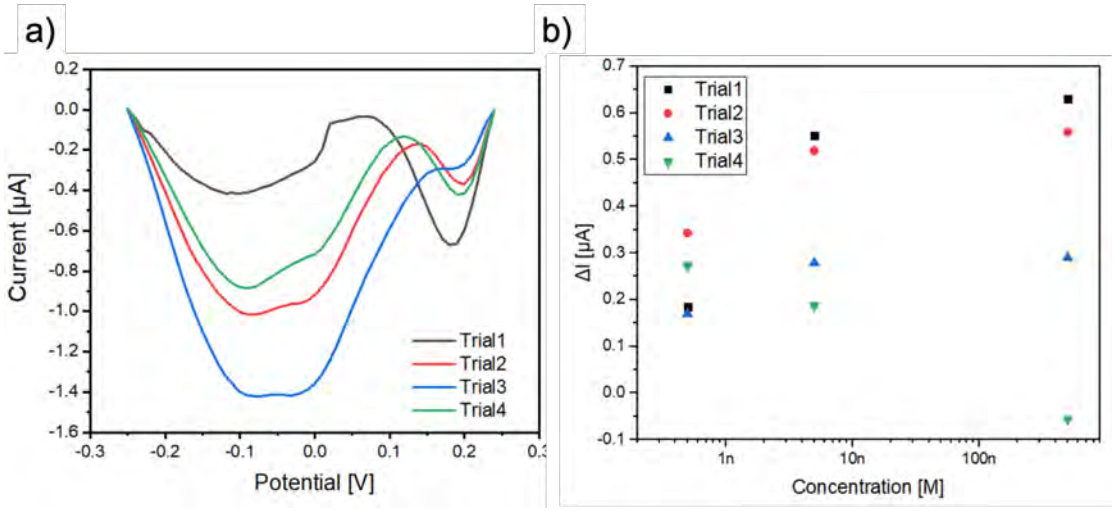

Figure 3.9. Studying the sensor lifetime and effect of sample washing. a) The SWV signal in blank solution (PBS) in the presence of dissolved oxygen scan with samples cleaned in PBS (Trial 1-3) or 99% IPA and PBS (Trial 4), b) sensor response to 500μM, 5 nM, and 500 nM H_2O_2 in PBS with samples cleaned through Trial 1-4.

tests were conducted with all analytes individually in PBS. The range of potentials swept through is 0.25 V to -0.25 V for SWV at a frequency of 3 Hz and CV was performed as explained in Section 3.2.2.1. As seen in Fig.3.10, the response to 5 nM H_2O_2 is around 7.5 time larger than the response to interfering analytes (5nM and 5 mM of UA and AA).

3.2.2.6 Preliminary fabrication of an on-chip sensor

As stated in Section 3.1, one of our goals was to fabricate an on-chip sensor to detect H_2O_2 without using bulky counter and reference electrodes. The on-chip sensor would be fabricated on a borosilicate glass slide with different materials creating the three-electrode set-up, i.e. a working electrode (Pt), counter electrode (carbon (C) or silver (Ag)), and reference electrode (C). The general design of the electrodes is shown in Fig.3.11a. The counter electrode is the electrode on the left, it needed to be at least three times the size of the working electrode (middle electrode). The redox reaction current is not limited by the counter electrode area in this configuration. Platinum is used for the working electrode and for the contact pads needed to connect to the potentiometer. The reference electrode is on the right.

There are two parameters explored during this study. The materials and sizing of the electrode were studied. The characterization of the open circuit potential of the reference electrodes is shown in Appendix B. Once the parameters of the material characterization were completed, the whole chip was fabricated for testing. The first attempt of H_2O_2

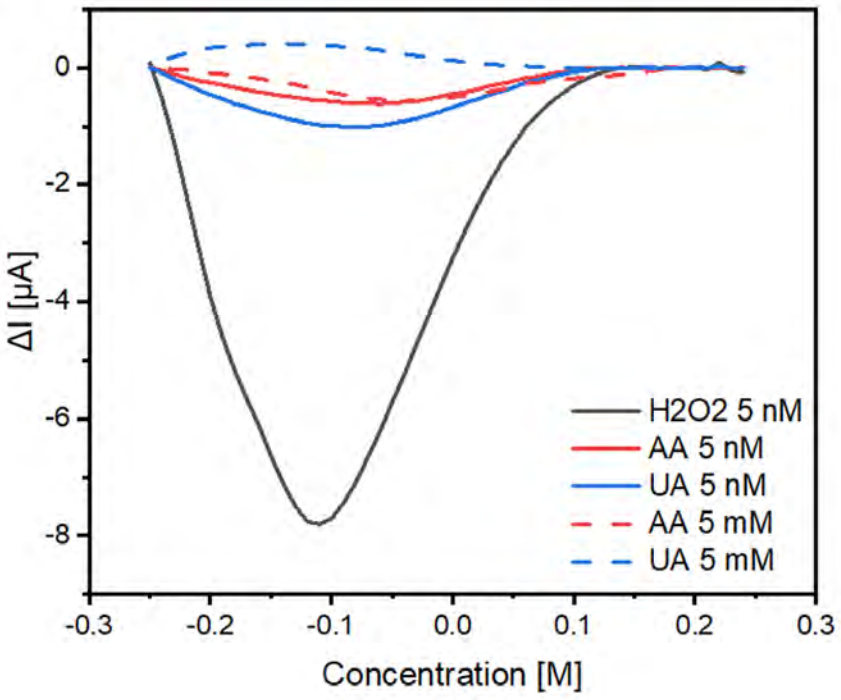

Figure 3.10. Studying the sensor response to interference. The tests were done in PBS on borosilicate glass and the curves are subtracted from a baseline.

testing was conducted with a RE of Ag, WE of Pt, and CE of C. There were stabilization problems with this configuration. As such, a standard RE (Ag/AgCl electrode) was introduced to the system, replacing the printed C reference electrode, as seen in Fig.3.11b. There were still stability problems. Instability was determined by a fluctuating OCP while trying to test and by failed connectivity tests of individual electrodes done with a digital multi-meter (DMM). To correct this, the second fabricated on-chip sensor was printed larger to help with the connectivity. Due to fabrication complications, the second sensor had a RE of C. This second sensor still had a fluctuating OCP and no connectivity. This is an area to further explore in the future.

Table 3.1 shows the comparison of this work to other non-enzymatic, Pt-based sensors. Almost all of the sensors were tested in PBS, similar to this work. The limit of detection for non-enzymatic sensors is normally in the nM-μM range which is at least eight orders of magnitude larger than the limit of detection observed here.

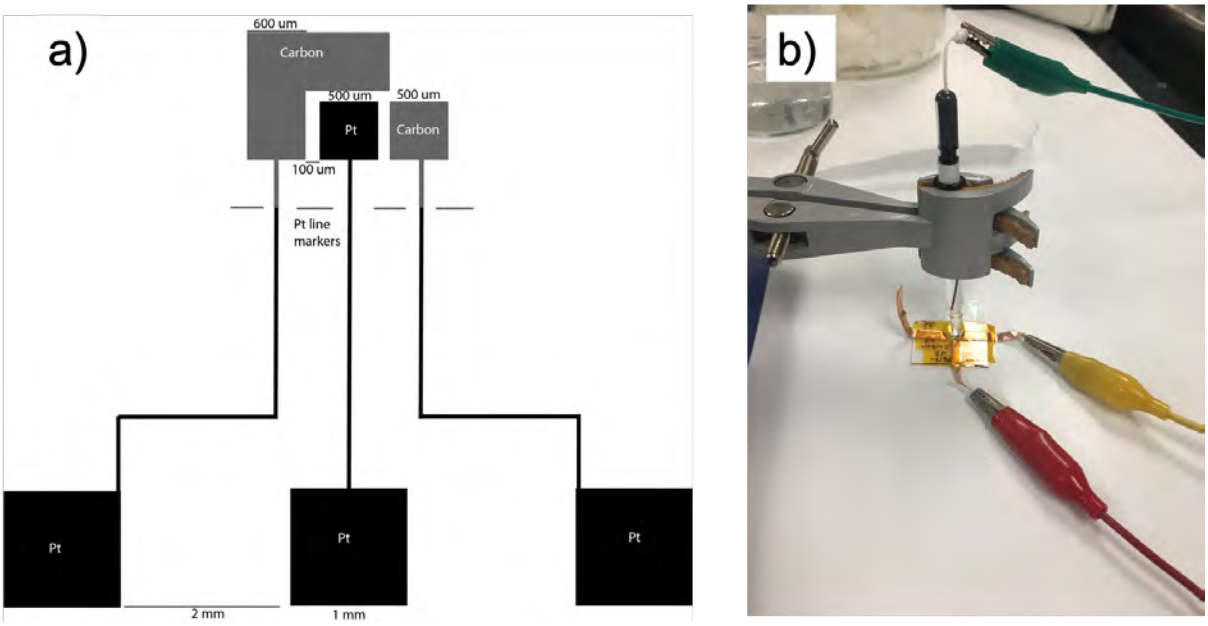

Figure 3.11. Studying on-chip fabrication a) The printer design of the chip and electrode dimension. b) The chip attached to a potentiostat.

3.3 Conclusion

In this work, we investigated the response of a recently developed laser writing Pt electrodes based on platinum salt precursor for developing a low-cost, disposable, and scalable electrochemical sensor for highly sensitive detection of hydrogen peroxide. The sensors demonstrate an ultra low detection limit of 5 fM in a buffer solution. We characterized the material using XPS and SEM to confim the presence of Pt and the morphology of the Pt electrodes. The effect of salt concentration on sensitivity was studied. Different substrates (FTO and borosilicate glass) were tested for the on-chip sensor. The lifetime of samples was studied with the conclusion that the samples are are suitable as disposable test electrodes (as with commercial glucose test strips). The future works entail developing a fully-printed on-chip sensor to detect H_2O_2. Future studies include the post-deposition treatment (such as annealing or plasma treatment) to possibly make the samples multi-use instead of single-use. By expanding the choice of the salt precursor, in future, sensors for other small molecules can be also investigated.

Material	Dynamic Range	Limit of Detection	Applied Potential	Medium	Ref
PPy/Pt/GCE	25–500 µM 500–6300 µM	0.6 µM	0.175 V	N_2-sat PBS	[80]
RGO-PT-Pt NPs/SPCEs	1.0–100.0 µM	0.6 µM	0.4 V	PBS	[32]
Pt-N-graphene/ ITO	0.001–1 mM	0.34 µM	0.40 V	0.1 M PBS	[70]
Nafion/Pt NPs/ RGO	5–3000 µM	0.4 µM	0.5 mV	0.1 M PBS	[83]
GCE/$PtTe_2$	3–300 µM 500–1100 µM	1.2 µM	0.25 V	N_2-sat PBS	[59]
Pt-MoS_2/GCE	0.004–48.5 mM	1 µM	0.05 V	N_2-sat PBS	[21]
$Pt_{0.5}Au_{0.5}$@C	0.007–6.5 mM	2.4 µM	0.3 V	0.1 M phosphate buffer solution	[60]
PtNPs@SPCE	0.001–1 mM	0.19 µM	0.7 V	phosphate buffer	[4]
CNF-PtNP	10 µM - 9.38 mM 9.38 - 74.38 mM	1.9 µM	0.34 V vs. SCE	0.1 M PBS	[39]
RGO/CS/ Fc/Pt/GE	0.00002–0.003 mM 0.006–10 mM	0.02 µM	0.05	PBS	[6]
GCE/Pt nanowire	5 µM - 3 mM	9.6 µM	0 V	0.1 M PBS	[74]
LW-Pt	5 fM – 50 nM	5 fM	-0.1 V	PBS	This work

Table 3.1. Comparable H_2O_2 sensors are listed displaying various characteristics of each sensor.NPs: nanoparticles, SPCE: screen-printed carbon electrodes , GCE: glassy carbon electrode, RGO: reduced graphene oxide, CNF: nanoporous carbon nanofibers, ITO: indium tin oxide, PPy: polypyrrole, N_2-sat: nitrogen saturated.

Chapter 4
Summary and Future Work

In summary, we explored two different materials as low-cost, scalable methods for PoC biosensing. The PBS-Cu-Ni material is able to detect glucose in neutral pH down to 5 nM of glucose. To the best of our knowledge, this is one of the few materials with ability to operate in neutral pH using transition metals. We studied various annealing and stabilization conditions to optimize the response. This optimization involves in a two-step annealing process. The annealing helped stabilize the copper by forming copper oxide and create a more homogeneous surface as seen in the XPS and EDS results. The sensors response to glucose was more stable and more sensitive when stabilized in PBS. The material showed good selectivity since glucose could still be detected while being in artificial saliva spiked with biologically-relevant concentrations of ascorbic acid and uric acid.

The future of this work is to try fabrication of the electrodes on other substrates to create a complete on-chip sensor. Some potential materials to study are laser-induced graphene (LIG) on polyimide sheets. This would be of interest to study because of the inherent flexibility of LIG. Another area of study could be to incorporate anti-fouling techniques. The PBS-Cu-Ni could selectively detect glucose in artificial saliva, but the solution needed to be diluted down to 3% into Na_2SO_4. Potential anti-fouling techniques include physical modifications and chemical modifications. Physical modifications include adsorption, mechanical coatings, and nanoporous structures. [41] Chemical modifications include self-assembling monolayers (SAM) and and polymer brushes. [41]

The second material is LWM-Pt. This is a new way of fabrication of Pt with a very porous, high active area. We are able to reliably reproduce a limit of detection of 5 fM in PBS. The effect of various Pt salt concentration was studied. With a Pt salt concentration of 0.25 M a high sensitivity even with the different substrates (non-FTO and FTO glass) can be achieved. The shift in baseline during testing on different days or

on the same day despite simple rinsing indicates a single-use sample. The laser writing process is scalable since even as the expose sample area decreases, the detection limit is still 5 fM. The sensor signal can be enhanced by choosing an optimum SWV frequency. The stability of laser written carbon (C) and silver (Ag) was also studied in an effort to create on-chip pseudo-reference electrode. They both are stable, with OCP fluctuation less than 10 mV.

More complex background can be studied in future such as artificial saliva, sweat, or urine. Post-deposition treatments could be of studied to improve the sensor lifetime. On-chip sensing is another topic to study. If an on-chip sensor with all 3 electrodes (WE, CE, RE) can be fabricated, this could have many applications in PoC devices to study cell metabolism or indirectly measure the response of enzymatic reactions. In addition, different laser written materials can be printed for testing other small molecules. Further studies are needed.

Appendix A
Optimization of the Processing Steps for Developing PBS-Cu-Ni Electrodes

While conducting tests, it was noticed that the signal seemed to decrease as more CV sweeps were done. It appeared that the copper was being stripped off the surface of the electrodes. This was confirmed by optical observations using a microscope. As seen in Fig. A.1.

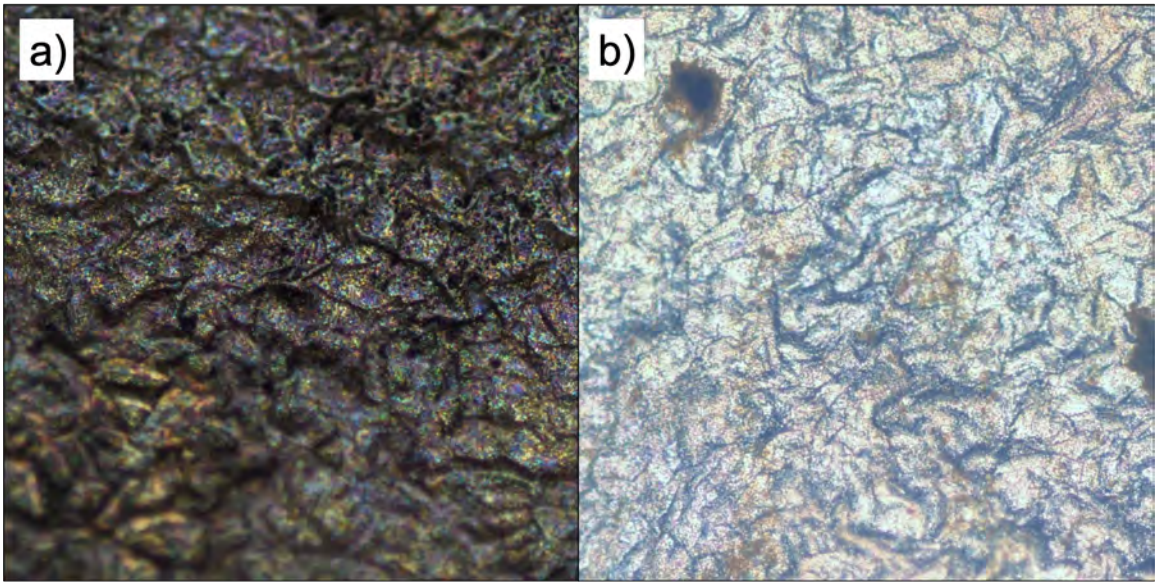

Figure A.1. a) Electrodeposited Cu-Ni before testing. b) Electrodeposited Cu-Ni after testing.

We studied the effect of various annealing and processing conditions on the electrodeposited samples (summmarized in Fig. A.2a).

The results shown in Fig. A.2b suggest that without PBS treatment, the sensor response is poor (timeline T2).PBS was introduced into the timeline T2P as PBS and copper can create phosphate-copper nanoflowers as discussed in Section 2.2.4.

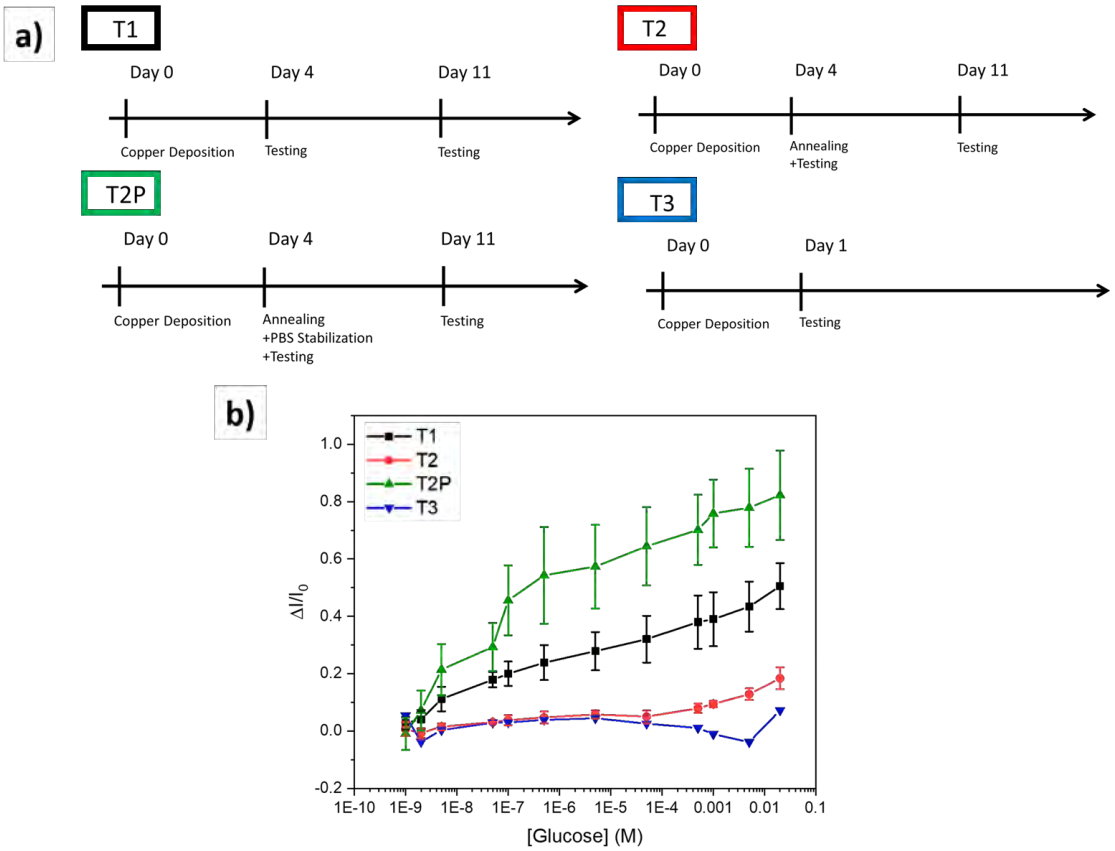

Figure A.2. a) The various timelines tested. Annealing was done at 150°C. b) The response in comparison of the different timelines on Day 4 testing in Na_2SO_4

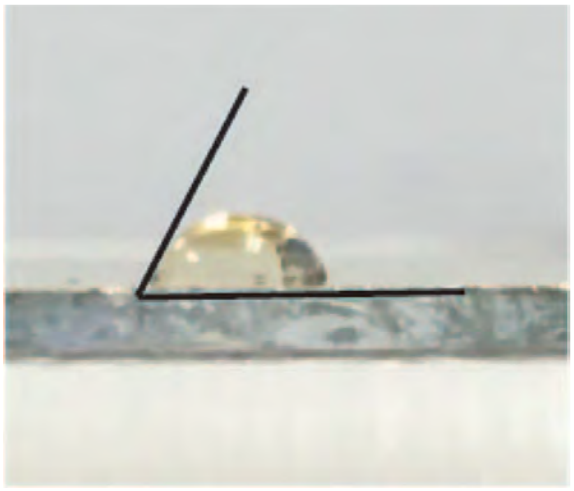

Figure A.3. Water on PBS-Cu-Ni 5 µL of water dropped on the surface.

The hydrophobicity of samples was also studied. Fig.A.3 shows the contact angle of the water is less than 90°making the material hydrophilic. Ideally, the more hydrophilic a surface is, the more resilient it would be against fouling. Hence, to improve antifouling properties of the samples further research needs to be done, for example coating the electrodes with specific polymers or other chemical/physical treatments. [41]

Appendix B
Characterization of Laser-written Silver and Carbon Pseudo Reference Electrodes

In the Chapter 3, we focused our efforts on studying Pt as the working electrode for electrochemical sensing of H2O2. To demonstrate the potential of the LWM process to create a fully-printed sensor with all necessary electrodes (working electrode, reference electrode, and counter electrode) integrated on the same substrate, we explored LWMs to create counter electrode and pseudo-reference electrode. To check if a material is suitable as a reference electrode, the open circuit potential (OCP) between the material and a known, standard reference electrode (such as glass Ag/AgCl reference electrode used in the previous sections) is measured in a highly conductive medium (such as 3M KCl). A stable (variation < 10 mV) open circuit potential is a necessary characteristic of a pseudo reference electrode.

Ag/AgCl is a very common reference electrode because it is very stable and it is environmentally friendly in comparison to Hg/Hg_2Cl_2, calomel electrode, and Tl(Hg)/TlCl. [67] With this in mind, the first material we tested was printed Ag on FTO glass. Ag was printed using a precursor containing $AgNO_3$. All measurements are conducted in 3M KCl for 40 minutes versus to the glass Ag/AgCl reference electrode.

Initially, the Ag would not adhere to the glass when written Ag onto normal (non-FTO) borosilicate glass. As such, printed carbon (C) was tested on normal glass. Carbon electrode was created by using Benzyl Benzoate as the precursor. This was also tested in 3M KCl for 40 minutes in comparison to the glass Ag/AgCl reference electrode as shown in Fig. B.1a.

We noticed the age of the Ag solution is important (perhaps due to possible oxidation

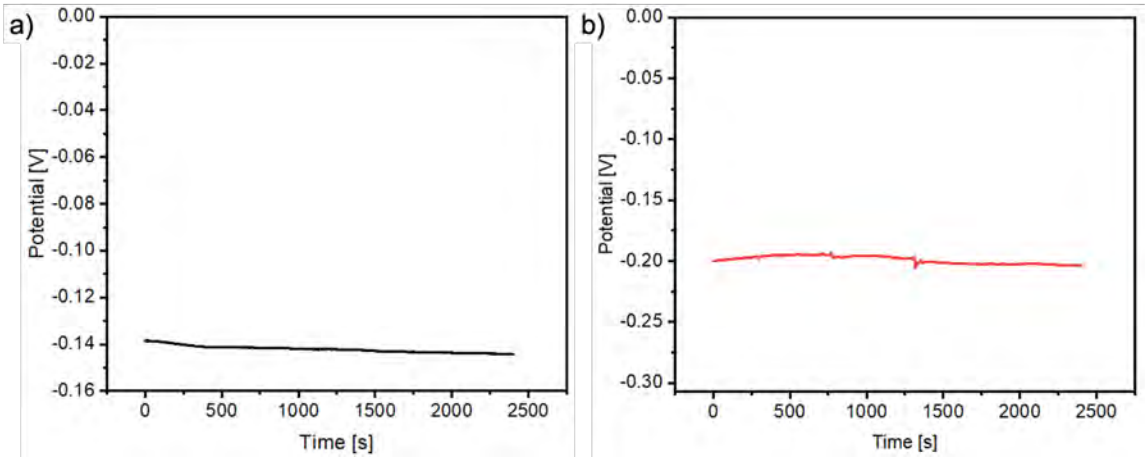

Figure B.1. The OCP laser-written C and Ag non-FTO glass. Mean, standard deviation, and standard error applies to the whole scan.

of the precursor with old reagents). By using fresh Ag suspension, the Ag film adhered well to non-FTO glass. The response of this is shown in Fig. B.1b.

Overall, the Ag and C stabilize over time in comparison to a standard Ag/AgCl. The next steps would be to fabricate the full on-chip sensor.

Bibliography

[1] P. U. Abel and T. Von Woedtke. Biosensors for in vivo glucose measurement: Can we cross the experimental stage. *Biosensors and Bioelectronics*, 17(11-12):1059–1070, 12 2002.

[2] Heba Abunahla, Baker Mohammad, Anas Alazzam, Maguy Abi Jaoude, Mahmoud Al-Qutayri, Sabina Abdul Hadi, and Said F. Al-Sarawi. MOMSense: Metal-Oxide-Metal Elementary Glucose Sensor. *Scientific Reports*, 9(1):1–10, 12 2019.

[3] Muhammad Adeel, Md Mahbubur Rahman, Isabella Caligiuri, Vincenzo Canzonieri, Flavio Rizzolio, and Salvatore Daniele. Recent advances of electrochemical and optical enzyme-free glucose sensors operating at physiological conditions. *Biosensors and Bioelectronics*, 165:112331, 5 2020.

[4] Jerónimo Agrisuelas, María Isabel González-Sánchez, and Edelmira Valero. Hydrogen peroxide sensor based on in situ grown Pt nanoparticles from waste screen-printed electrodes. *Sensors and Actuators, B: Chemical*, 249:499–505, 10 2017.

[5] Xiaofang Bai, Wei Chen, Yanfang Song, Jiazhou Zhang, Ruipeng Ge, Wei Wei, Zheng Jiao, and Yuhan Sun. Nickel-copper oxide nanowires for highly sensitive sensing of glucose. *Applied Surface Science*, 420:927–934, 10 2017.

[6] Zhihao Bai, Guiyin Li, Jingtao Liang, Jing Su, Yue Zhang, Huaizhou Chen, Yong Huang, Weiguo Sui, and Yongxiang Zhao. Non-enzymatic electrochemical biosensor based on Pt NPs/RGO-CS-Fc nano-hybrids for the detection of hydrogen peroxide in living cells. *Biosensors and Bioelectronics*, 82:185–194, 8 2016.

[7] Saikat Banerjee, Md Faruk Hossain, and Gymama Slaughter. A Highly Sensitive Non-Enzymatic Hydrogen Peroxide Sensor based on Palladium-Gold Nanoparticles. In *2020 IEEE 15th International Conference on Nano/Micro Engineered and Molecular System (NEMS)*, pages 286–289. IEEE, 9 2020.

[8] Allen Bard and Larry Faulkner. *Electrochemical Methods: Fundamentals and Applications*. John Wiley & Sons, Inc., Danvers, 2 edition, 2001.

[9] P. M. Biesheuvel, S. Porada, and J. E. Dykstra. The difference between faradaic and non-faradaic electrode processes, 2021.

[10] Adam Bolotsky, Derrick Butler, Chengye Dong, Katy Gerace, Nicholas R. Glavin, Christopher Muratore, Joshua A. Robinson, and Aida Ebrahimi. Two-Dimensional Materials in Biosensing and Healthcare: From In Vitro Diagnostics to Optogenetics and Beyond. *ACS Nano*, 13(9):9781–9810, 5 2019.

[11] Fei Cao, Shu Guo, Huiyan Ma, Guocheng Yang, Shengxue Yang, and Jian Gong. Highly sensitive nonenzymatic glucose sensor based on electrospun copper oxide-doped nickel oxide composite microfibers. *Talanta*, 86(1):214–220, 10 2011.

[12] Mohamed Lyamine Chelaghmia, Mouna Nacef, Abed Mohamed Affoune, Maxime Pontié, and Tahar Derabla. Facile Synthesis of Ni(OH) ₂ Modified Disposable Pencil Graphite Electrode and its Application for Highly Sensitive Non-enzymatic Glucose Sensor. *Electroanalysis*, 30(6):1117–1124, 6 2018.

[13] Shihong Chen, Ruo Yuan, Yaqin Chai, and Fangxin Hu. Electrochemical sensing of hydrogen peroxide using metal nanoparticles: A review. *Microchimica Acta*, 180(1-2):15–32, 11 2013.

[14] Niancai Cheng, Samantha Stambula, Da Wang, Mohammad Norouzi Banis, Jian Liu, Adam Riese, Biwei Xiao, Ruying Li, Tsun Kong Sham, Li Min Liu, Gianluigi A. Botton, and Xueliang Sun. Platinum single-atom and cluster catalysis of the hydrogen evolution reaction. *Nature Communications*, 7(1):1–9, 11 2016.

[15] David B. Cordes, Aaron Miller, Soya Gamsey, Zach Sharrett, Praveen Thoniyot, Ritchie Wessling, and Bakthan Singaram. Optical glucose detection across the visible spectrum using anionic fluorescent dyes and a viologen quencher in a two-component saccharide sensing system. *Organic and Biomolecular Chemistry*, 3(9):1708–1713, 5 2005.

[16] David B. Cordes, Aaron Miller, Soya Gamsey, and Bakthan Singaram. Simultaneous use of multiple fluorescent reporter dyes for glucose sensing in aqueous solution. *Analytical and Bioanalytical Chemistry*, 387(8):2767–2773, 4 2007.

[17] Everson T.S.G. da Silva, Dênio E.P. Souto, José T.C. Barragan, Juliana de F. Giarola, Ana C.M. de Moraes, and Lauro T. Kubota. Electrochemical Biosensors in Point-of-Care Devices: Recent Advances and Future Trends, 4 2017.

[18] Pavel Damborský, Juraj Švitel, and Jaroslav Katrlík. Optical biosensors. *Essays in Biochemistry*, 60(1):91–100, 6 2016.

[19] S. Darvishi, M. Souissi, F. Karimzadeh, M. Kharaziha, R. Sahara, and S. Ahadian. Ni nanoparticle-decorated reduced graphene oxide for non-enzymatic glucose sensing: An experimental and modeling study. *Electrochimica Acta*, 240:388–398, 6 2017.

[20] Keerthy Dhara and Debiprosad Roy Mahapatra. Recent advances in electrochemical nonenzymatic hydrogen peroxide sensors based on nanomaterials: a review, 10 2019.

[21] Kaiyue Duan, Yongling Du, Qingliang Feng, Xiaoliang Ye, Hong Xie, Muyin Xue, and Chunming Wang. Synthesis of Platinum Nanoparticles by using Molybdenum Disulfide as a Template and its Application to Enzyme-like Catalysis. *ChemCatChem*, 6(7):1873–1876, 7 2014.

[22] Cheng Fang, Chenglin Yi, Yang Wang, Yuhua Cao, and Xiaoya Liu. Electrochemical sensor based on molecular imprinting by photo-sensitive polymers. *Biosensors and Bioelectronics*, 24(10):3164–3169, 6 2009.

[23] Linxia Fang, Fan Wang, Zhenghua Chen, Yan Qiu, Tianli Zhai, Mengmeng Hu, Cuijie Zhang, and Kejing Huang. Flower-like MoS2 decorated with Cu2O nanoparticles for non-enzymatic amperometric sensing of glucose. *Talanta*, 167:593–599, 5 2017.

[24] Shuai Fu, Guoli Fan, Lan Yang, and Feng Li. Non-enzymatic glucose sensor based on Au nanoparticles decorated ternary Ni-Al layered double hydroxide/single-walled carbon nanotubes/graphene nanocomposite. *Electrochimica Acta*, 152:146–154, 1 2015.

[25] Kh Ghanbari and Z. Babaei. Fabrication and characterization of non-enzymatic glucose sensor based on ternary NiO/CuO/polyaniline nanocomposite. *Analytical Biochemistry*, 498:37–46, 4 2016.

[26] Lindsey Goodnight, Derrick Butler, and Aida Ebrahimi. Non-Enzymatic Detection of Glucose in Neutral pH using PBS-Activated Cu-Ni Electrodes . In *Materials Day*, 2020.

[27] Chunyan Guo, Yinmei Wang, Yongqing Zhao, and Cailing Xu. Non-enzymatic glucose sensor based on three dimensional nickel oxide for enhanced sensitivity. *Analytical Methods*, 5(7):1644–1647, 4 2013.

[28] Shreya Gupta, Meghanand Nayak, J. Sunitha, Geetanshu Dawar, Nidhi Sinha, and Neelakshi Rallan. Correlation of salivary glucose level with blood glucose level in diabetes mellitus. *Journal of Oral and Maxillofacial Pathology*, 21(3):334–339, 9 2017.

[29] Shokoufeh Hassani, Saeideh Momtaz, Faezeh Vakhshiteh, Armin Salek Maghsoudi, Mohammad Reza Ganjali, Parviz Norouzi, and Mohammad Abdollahi. Biosensors and their applications in detection of organophosphorus pesticides in the environment, 1 2017.

[30] Guangli He, Weihua Hu, and Chang Ming Li. Spontaneous interfacial reaction between metallic copper and PBS to form cupric phosphate nanoflower and its enzyme hybrid with enhanced activity. *Colloids and Surfaces B: Biointerfaces*, 135:613–618, 11 2015.

[31] Sijing He, Zuanguang Chen, Yanyan Yu, and Lijuan Shi. A novel non-enzymatic hydrogen peroxide sensor based on poly-melamine film modified with platinum nanoparticles. *RSC Advances*, 4(85):45185–45190, 9 2014.

[32] Yong Huang, Yewei Xue, Junxiang Zeng, Shanshan Li, Zhihong Wang, Chenyang Dong, Guiyin Li, Jintao Liang, and Zhide Zhou. Non-enzymatic electrochemical hydrogen peroxide biosensor based on reduction graphene oxide-persimmon tannin-platinum nanocomposite. *Materials Science and Engineering C*, 92:590–598, 11 2018.

[33] G. Jönsson and L. Gorton. An electrochemical sensor for hydrogen peroxide based on peroxidase adsorbed on a spectrographic graphite electrode. *Electroanalysis*, 1(5):465–468, 9 1989.

[34] Xinhuang Kang, Zhibin Mai, Xiaoyong Zou, Peixiang Cai, and Jinyuan Mo. A sensitive nonenzymatic glucose sensor in alkaline media with a copper nanocluster/-multiwall carbon nanotube-modified glassy carbon electrode. *Analytical Biochemistry*, 363(1):143–150, 4 2007.

[35] Ioannis Katsounaros, Wolfgang B. Schneider, Josef C. Meier, Udo Benedikt, P. Ulrich Biedermann, Alexander A. Auer, and Karl J.J. Mayrhofer. Hydrogen peroxide electrochemistry on platinum: Towards understanding the oxygen reduction reaction mechanism. *Physical Chemistry Chemical Physics*, 14(20):7384–7391, 5 2012.

[36] Heidi E. Koschwanez and William M. Reichert. In vitro, in vivo and post explantation testing of glucose-detecting biosensors: Current methods and recommendations, 9 2007.

[37] Saram Lee, Joungmin Lee, Sejin Park, Hankil Boo, Hee Chan Kim, and Taek Dong Chung. Disposable non-enzymatic blood glucose sensing strip based on nanoporous platinum particles. *Applied Materials Today*, 10:24–29, 3 2018.

[38] Xiaoling Li, Jianyu Yao, Feila Liu, Huichao He, Ming Zhou, Nan Mao, Peng Xiao, and Yunhuai Zhang. Nickel/Copper nanoparticles modified TiO2 nanotubes for non-enzymatic glucose biosensors. *Sensors and Actuators, B: Chemical B: Chemical*, 181:501–508, 5 2013.

[39] Yang Li, Mingfa Zhang, Xiaopeng Zhang, Guocheng Xie, Zhiqiang Su, and Gang Wei. Nanoporous Carbon Nanofibers Decorated with Platinum Nanoparticles for Non-Enzymatic Electrochemical Sensing of H2O2. *Nanomaterials*, 5(4):1891–1905, 11 2015.

[40] Kuo-Chiang Lin, Yu-Ching Lin, and Shen-Ming Chen. A highly sensitive nonenzymatic glucose sensor based on multi-walled carbon nanotubes decorated with nickel and copper nanoparticles. *Electrochimica Acta*, 96:164–172, 4 2013.

[41] Pei-Heng Lin and Bor-Ran Li. Antifouling strategies in advanced electrochemical sensors and biosensors. *Analyst*, 145(4):1110–1120, 2 2020.

[42] Sen Liu, Bo Yu, and Tong Zhang. A novel non-enzymatic glucose sensor based on NiO hollow spheres. 102:104–107, 7 2013.

[43] Jing Luo, Sisi Jiang, Hongyan Zhang, Jinqiang Jiang, and Xiaoya Liu. A novel non-enzymatic glucose sensor based on Cu nanoparticle modified graphene sheets electrode. *Analytica Chimica Acta*, 709:47–53, 1 2012.

[44] Soliman A Mahmoud, Heba A Salem, and Hend M Albalooshi. An 8-bit, 10 KS/s, Successive Approximation Analog to Digital Converter in CMOS Technology for

ECG Detection Systems. *Circuits, Systems, and Signal Processing*, 34:2419–2439, 2015.

[45] Keith B. Male, Sabahudin Hrapovic, Yali Liu, Dashan Wang, and John H.T. Luong. Electrochemical detection of carbohydrates using copper nanoparticles and carbon nanotubes. *Analytica Chimica Acta*, 516(1-2):35–41, 7 2004.

[46] Parikha Mehrotra. Biosensors and their applications - A review, 5 2016.

[47] Guilherme P.C. C. Mello, Eliana F.C. C. Simões, Diana M.A. A. Crista, João M.M. M. Leitão, Luís Pinto da Silva, and Joaquim C.G. G. Esteves da Silva. Glucose Sensing by Fluorescent Nanomaterials. *Critical Reviews in Analytical Chemistry*, 49(6):542–552, 11 2019.

[48] Feihong Meng, Wei Shi, Yanan Sun, Xuan Zhu, Guisen Wu, Changqing Ruan, Xin Liu, and Dongtao Ge. Nonenzymatic biosensor based on CuxO nanoparticles deposited on polypyrrole nanowires for improving detection range. *Biosensors and Bioelectronics*, 42(1):141–147, 4 2013.

[49] Ahmad Reza Mohamadi, Navabeh Nami, and Banafsheh Norouzi. Bio-directed synthesis of platinum nanoparticles by Nymphaea alba extract: fabrication of a novel non-enzymatic hydrogen peroxide sensor. *Journal of Materials Science: Materials in Electronics*, 31(21):18721–18731, 10 2020.

[50] Mouna Nacef, Mohamed Lyamine Chelaghmia, Abed Mohamed Affoune, and Maxime Pontié. Electrochemical Investigation of Glucose on a Highly Sensitive Nickel-Copper Modified Pencil Graphite Electrode. *Electroanalysis*, 31(1):113–120, 1 2019.

[51] Craig J. Neal, Ankur Gupta, Swetha Barkam, Shashank Saraf, Soumen Das, Hyoung J. Cho, and Sudipta Seal. Picomolar Detection of Hydrogen Peroxide using Enzyme-free Inorganic Nanoparticle-based Sensor. *Scientific Reports*, 7(1), 12 2017.

[52] X. H. Niu, L. B. Shi, H. L. Zhao, and M. B. Lan. Advanced strategies for improving the analytical performance of Pt-based nonenzymatic electrochemical glucose sensors: A minireview, 2 2016.

[53] Xiangheng Niu, Xin Li, Jianming Pan, Yanfang He, Fengxian Qiu, and Yongsheng Yan. Recent advances in non-enzymatic electrochemical glucose sensors based on non-precious transition metal materials: Opportunities and challenges, 9 2016.

[54] S. J. Padayatty and M. Levine. Vitamin C: the known and the unknown and Goldilocks, 2016.

[55] Sejin Park, Hankil Boo, and Taek Dong Chung. Electrochemical non-enzymatic glucose sensors, 1 2006.

[56] V Pockevicius, V Markevicius, M Cepenas, D Andriukaitis, and D Navikas. Blood Glucose Level Estimation Using Interdigital Electrodes. pages 7–10, 2013.

[57] Md. Mahbubur Rahman, A. J. Saleh Ahammad, Joon-Hyung Jin, Sang Jung Ahn, and Jae-Joon Lee. A Comprehensive Review of Glucose Biosensors Based on Nanostructured Metal-Oxides. *Sensors*, 10(5):4855–4886, 5 2010.

[58] Gérard Reach and S. Wilson George. Can Continuous Glucose Monitoring Be Used for the Treatment of Diabetes ? 64(6):381–386, 1992.

[59] Nasuha Rohaizad, Carmen C. Mayorga-Martinez, Zdeněk Sofer, Richard D. Webster, and Martin Pumera. Layered platinum dichalcogenides (PtS2, PtSe2, PtTe2) for non-enzymatic electrochemical sensor. *Applied Materials Today*, 19:100606, 6 2020.

[60] Ozlem Gokdogan Sahin. Microwave-assisted synthesis of PtAu@C based bimetallic nanocatalysts for non-enzymatic H2O2 sensor. *Electrochimica Acta*, 180:873–878, 10 2015.

[61] Masanori Seki, Ken Ichiro Iida, Mitsumasa Saito, Hiroaki Nakayama, and Shin Ichi Yoshida. Hydrogen Peroxide Production in Streptococcus pyogenes: Involvement of Lactate Oxidase and Coupling with Aerobic Utilization of Lactate. *Journal of Bacteriology*, 186(7):2046–2051, 4 2004.

[62] Rui Serra-Maia, Marion Bellier, Stephen Chastka, Kevin Tranhuu, Andrew Subowo, J. Donald Rimstidt, Pavel M. Usov, Amanda J. Morris, and F. Marc Michel. Mechanism and Kinetics of Hydrogen Peroxide Decomposition on Platinum Nanocatalysts. *ACS Applied Materials and Interfaces*, 10(25):21224–21234, 6 2018.

[63] Luba Shabnam, Shaikh Nayeem Faisal, Anup Kumar Roy, Enamul Haque, Andrew I. Minett, and Vincent G. Gomes. Doped graphene/Cu nanocomposite: A high sensitivity non-enzymatic glucose sensor for food. *Food Chemistry*, 221:751–759, 4 2017.

[64] Wenchao Sheng, Hubert A. Gasteiger, and Yang Shao-Horn. Hydrogen Oxidation and Evolution Reaction Kinetics on Platinum: Acid vs Alkaline Electrolytes. *Journal of The Electrochemical Society*, 157(11):B1529, 9 2010.

[65] Koichi Shibasaki, Masatoshi Kimura, Ryuichi Ikarashi, Akira Yamaguchi, and Takuya Watanabe. Uric acid concentration in saliva and its changes with the patients receiving treatment for hyperuricemia. *Metabolomics*, 8(3):484–491, 6 2012.

[66] Kyubin Shim, Won Chul Lee, Min Sik Park, Mohammed Shahabuddin, Yusuke Yamauchi, Md Shahriar A. Hossain, Yoon Bo Shim, and Jung Ho Kim. Au decorated core-shell structured Au@Pt for the glucose oxidation reaction. *Sensors and Actuators, B: Chemical*, 278:88–96, 1 2019.

[67] Marios Sophocleous and John K. Atkinson. A review of screen-printed silver/silver chloride (Ag/AgCl) reference electrodes potentially suitable for environmental potentiometric sensors, 11 2017.

[68] Shin Soyoon, Ananthakumar Ramadoss, Balasubramaniam Saravanakumar, and Sang Jae Kim. Novel Cu/CuO/ZnO hybrid hierarchical nanostructures for non-enzymatic glucose sensor application. 717-718:90–95, 3 2014.

[69] Mark Steven Steiner, Axel Duerkop, and Otto S. Wolfbeis. Optical methods for sensing glucose. *Chemical Society Reviews*, 40(9):4805–4839, 8 2011.

[70] M. T. Tajabadi, M. Sookhakian, E. Zalnezhad, G. H. Yoon, A. M.S. Hamouda, Majid Azarang, W. J. Basirun, and Y. Alias. Electrodeposition of flower-like platinum on electrophoretically grown nitrogen-doped graphene as a highly sensitive electrochemical non-enzymatic biosensor for hydrogen peroxide detection. *Applied Surface Science*, 386:418–426, 11 2016.

[71] Kathryn E. Toghill and Richard G. Compton. No Title. 2010.

[72] Robert Turner. Intensive blood-glucose control with sulphonylureas or insulin compared with conventional treatment and risk of complications in patients with type 2 diabetes (UKPDS 33). *Lancet*, 352(9131):837–853, 9 1998.

[73] Bin Wang, Yuanya Wu, Yanfen Chen, Bo Weng, and Changming Li. Flexible paper sensor fabricated via in situ growth of Cu nanoflower on RGO sheets towards amperometrically non-enzymatic detection of glucose. *Sensors and Actuators, B: Chemical*, 238:802–808, 1 2017.

[74] Shuqi Wang, Li Ping Xu, Hai Wei Liang, Shu Hong Yu, Yongqiang Wen, Shutao Wang, and Xueji Zhang. Self-interconnecting Pt nanowire network electrode for electrochemical amperometric biosensor. *Nanoscale*, 7(26):11460–11467, 7 2015.

[75] Xiaojie Wang, Qian Wu, Kaili Jiang, Chuanxi Wang, and Chi Zhang. One-step synthesis of water-soluble and highly fluorescent MoS2 quantum dots for detection of hydrogen peroxide and glucose. *Sensors and Actuators, B: Chemical*, 252:183–190, 11 2017.

[76] P. Westbroek. Electrochemical methods. In *Analytical Electrochemistry in Textiles*, pages 37–69. Elsevier Inc., 1 2005.

[77] Y. Wickramasinghe, Y. Yang, and S. A. Spencer. Current problems and potential techniques in in vivo glucose monitoring. 14(5):513–520, 9 2004.

[78] R. Wilson and A. P.F. Turner. Glucose oxidase: an ideal enzyme, 1 1992.

[79] Otto S. Wolfbeis, Axel Dürkop, Meng Wu, and Zhihong Lin. A europium-ion-based luminescent sensing probe for hydrogen peroxide. *Angewandte Chemie - International Edition*, 41(23):4495–4498, 12 2002.

[80] Liwen Xing, Qinfeng Rong, and Zhanfang Ma. Non-enzymatic electrochemical sensing of hydrogen peroxide based on polypyrrole/platinum nanocomposites. *Sensors and Actuators, B: Chemical*, 221:242–247, 7 2015.

[81] Wei Yi, Juan Liu, Hongbiao Chen, Yong Gao, and Huaming Li. Copper/nickel nanoparticle decorated carbon nanotubes for nonenzymatic glucose biosensor. *Journal of Solid State Electrochemistry*, 19(5):1511–1521, 4 2015.

[82] Lauren D. Zarzar, B. S. Swartzentruber, Brian F. Donovan, Patrick E. Hopkins, and Bryan Kaehr. Using Laser-Induced Thermal Voxels to Pattern Diverse Materials at the Solid-Liquid Interface. *ACS Applied Materials and Interfaces*, 8(33):21134–21139, 8 2016.

[83] Cong Zhang, Haohai Jiang, Rui Ma, Yanyan Zhang, and Qiang Chen. Simple non-enzymatic electrochemical sensor for hydrogen peroxide based on nafion/platinum nanoparticles/reduced graphene oxide nanocomposite modified glassy carbon electrode. 2016.

[84] Yuchan Zhang, Liang Su, Dan Manuzzi, Honorio Valdés Espinosa de los Monteros, Wenzhao Jia, Danqun Huo, Changjun Hou, and Yu Lei. Ultrasensitive and selective non-enzymatic glucose detection using copper nanowires. *Biosensors and Bioelectronics*, 31(1):426–432, 1 2012.

[85] Jiang Zhao, Liangming Wei, Chonghao Peng, Yanjie Su, Zhi Yang, Liying Zhang, Hao Wei, and Yafei Zhang. A non-enzymatic glucose sensor based on the composite of cubic Cu nanoparticles and arc-synthesized multi-walled carbon nanotubes. 47:86–91, 9 2013.

[86] Anni Zhong, Xiaoli Luo, Liping Chen, Shanshan Wei, Yonghong Liang, and Xinchun Li. Enzyme-free sensing of glucose on a copper electrode modified with nickel nanoparticles and multiwalled carbon nanotubes. *Microchimica Acta*, 182(5-6):1197–1204, 12 2015.

[87] Juan Zhou, Yanan Zhao, Jing Bao, Danqun Huo, Huanbao Fa, Xin Shen, and Changjun Hou. One-step electrodeposition of Au-Pt bimetallic nanoparticles on MoS2 nanoflowers for hydrogen peroxide enzyme-free electrochemical sensor. *Electrochimica Acta*, 250:152–158, 10 2017.

[88] Hua Zhu, Li Li, Wei Zhou, Zongping Shao, and Xianjian Chen. Advances in non-enzymatic glucose sensors based on metal oxides, 11 2016.